FUNDAMENTAL STUDY OF COMPRESSIVE STRENGTH DEVELOPMENT IN PAN-BASED CARBON FIBERS

(2)

FINAL TECHNICAL REPORT

Prepared By

A.S. Abhiraman
Principal Investigator
Prashant Desai
Hao Jiang

Contract Number: AFOSR-89-0193
Sponsored by Air Force Office of Scientific Research

GEORGIA INSTITUTE OF TECHNOLOGY
Atlanta, GA 30332-0100

GEORGIA INSTITUTE OF TECHNOLOGY
A Unit of the University System of Georgia
Atlanta, Georgia 30332

Georgia Tech
RESEARCH INSTITUTE

UNCLASSIFIED
SECURITY CLASSIFICATION OF THIS PAGE

REPORT DOCUMENTATION PAGE

1a. REPORT SECURITY CLASSIFICATION: U	1b. RESTRICTIVE MARKINGS
2a. SECURITY CLASSIFICATION AUTHORITY	3. DISTRIBUTION/AVAILABILITY OF REPORT: unlimited
2b. DECLASSIFICATION/DOWNGRADING SCHEDULE	
4. PERFORMING ORGANIZATION REPORT NUMBER(S): E-19-642-4	5. MONITORING ORGANIZATION REPORT NUMBER(S)
6a. NAME OF PERFORMING ORGANIZATION: Ga. Tech Research Corporation; 6b. OFFICE SYMBOL (If applicable)	7a. NAME OF MONITORING ORGANIZATION: AFOSR
6c. ADDRESS (City, State, and ZIP Code): Ga. Tech Research Corp./Ga.Inst. of Technology, Centennial Res. Bldg., Rm. 24, Atlanta, GA 30332-0420	7b. ADDRESS (City, State, and ZIP Code): Lt. Col. Larry W. Burggraf, AFOSR/NC, Building 410, Bolling AFB, DC 20332-6448
8a. NAME OF FUNDING/SPONSORING ORGANIZATION: AFOSR; 8b. OFFICE SYMBOL (If applicable): NC	9. PROCUREMENT INSTRUMENT IDENTIFICATION NUMBER: AFOSR 89-0193
8c. ADDRESS (City, State, and ZIP Code): AFOSR/NC, Building 410, Bolling AFB, DC 20332-6448	10. SOURCE OF FUNDING NUMBERS

PROGRAM ELEMENT NO.	PROJECT NO.	TASK NO.	WORK UNIT ACCESSION NO.
61102F	2419	06	

11. TITLE (Include Security Classification): Fundamental Study of Compressive Strength Development in PAN-Based Carbon Fibers U

12. PERSONAL AUTHOR(S): A.S. Abhiraman

13a. TYPE OF REPORT	13b. TIME COVERED	14. DATE OF REPORT (Year, Month, Day)	15. PAGE COUNT
final	FROM 12/88 TO 9/91	920320	80

16. SUPPLEMENTARY NOTATION

17. COSATI CODES		
FIELD	GROUP	SUB-GROUP

18. SUBJECT TERMS (Continue on reverse if necessary and identify by block number): Carbon Fiber Formation, Recoil Strength, Compressive Strength, PBZT Fibers, PAN Fibers, MechanicalProperties of Carbon Fibers, Recoil Fracture Analysis

19. ABSTRACT (Continue on reverse if necessary and identify by block number)

Evolution of mechanical properties in the conversion of two precursor polymeric fibers to carbon fibers has been studied. The focus has been on properties in axial compression of polyacrylonitrile (PAN, a semi rigid polymer) - and polybenzobisthiazole (PBZT, a rigid rod polymer) - based carbon fibers. Mechanical properties of fibers at different extents of progression toward the graphite fiber structure reveal that the evolutions of tensile and compressive properties are not synchronized. Substantial enhancements in both tensile and compressive strengths of carbon fibers occur only with the development of the carbonized morphology with its characteristic basal planes as the fundmental structural units.

In addition, the "recoil from tension" method has been analyzed vis-a-vis axial compressive strength of carbon fibers. Fracture surfaces of specimens from this experiment do not necessarily reveal failure in a simple compression mode and especially includes bending. Statistical analysis of the recoil method demonstrates that the fiber failure distribution can be expressed by either a logistic or a Weibull distribution. However, a universal logistic distribution of recoil failure stresses,containing an interactive stress-gauge length (over)

20. DISTRIBUTION/AVAILABILITY OF ABSTRACT	21. ABSTRACT SECURITY CLASSIFICATION
☒ UNCLASSIFIED/UNLIMITED ☐ SAME AS RPT. ☐ DTIC USERS	UNCLASSIFIED

22a. NAME OF RESPONSIBLE INDIVIDUAL	22b. TELEPHONE (Include Area Code)	22c. OFFICE SYMBOL
Lt Col Burggraf	(202) 767-4960	AFOSR/NC

DD FORM 1473, 84 MAR — 83 APR edition may be used until exhausted. All other editions are obsolete.

SECURITY CLASSIFICATION OF THIS PAGE
UNCLASSIFIED

TABLE OF CONTENTS

ACKNOWLEDGMENTS

The authors express their appreciation to Mr. Sundar Damodaran (GT), Dr. Satish Kumar (GT), Dr. C. Y-C. Lee (Air Force Materials Laboratory), and Dr. Steve Smith (Courtaulds, UK), for useful discussions at various times preceding and during the course of the research project reported here.

Much of the design and construction of experimental accessories and acquisition of the data reported here were carried out by Mr. S. Damodaran, Ph. D. student, and Dr. Hao Jiang, Post-doctoral Fellow.

FUNDAMENTAL STUDY OF COMPRESSIVE STRENGTH DEVELOPMENT IN PAN BASED CARBON FIBERS

I. INTRODUCTION

The evolution of different organic and inorganic high performance fibers for applications in structural composites constitutes one of the most significant recent advances in materials science and engineering. These materials provide heretofore unmatched specific mechanical performance, especially in tension. However, applications of these structural materials are limited by, among other things, their relatively inferior performance in compression. With the exception of a few fibers, such as boron, the best axial compressive strength which has been achieved is less than 25% of the best axial tensile strength of most of these fibers. It is therefore necessary to identify the mechanisms responsible for limiting the compressive strength of high performance fibers and effect the necessary changes in the formation of these fibers to enhance it. The variety of structures which are created in the formation of carbon fibers and the associated broad range of properties in tension and compression make them ideally suited for this purpose.

II. OBJECTIVES

The primary objective of the current project is to generate the necessary fundamental knowledge regarding structure and compressive strength of carbon fibers. A study of the evolution of morphology and compressive properties in the formation of carbon fibers from polyacrylonitrile (PAN)-based precursor polymers constitutes the major component in this effort. The chemical and morphological structures that are obtained through the gradual conversion of fibers of intrinsically semi-rigid PAN-based linear polymers to the rigid plate-like structure of the basal planes in the carbon/graphite fibers offer an ideal sequence of materials for this purpose. The ultimate goal here is to use this knowledge to guide material and process developments to achieve superior compressive strength in fibers, especially in fibers of rigid rod organic polymers, so that a significantly higher level of benefit can be realized from the recent advances in achieving high tensile performance.

Major efforts in this project have been directed toward (i) analysis of the recoil test for the measurement of compressive strength of carbon fibers; (ii) verification of the suitability of the recoil test for evaluations of the fibers from (iii); (iii) generation of fiber samples at different stages in the evolution of the carbonized fiber morphology; and (iv) exploration of mechanisms by which different carbon fiber morphologies can be generated.

Significant progress has been made in every component of this

investigation. Conclusive results pertaining to (i)–(iii) have been obtained. A reduction in the effort (from that in the original proposal) led to the work regarding (iv) being limited to preliminary exploratory studies. The procedures for – and the results from – these investigations are summarized in Section III. The conclusions and recommendations are given in Section IV. Detailed accounts of the research are given in the Appendices via reprints/preprints of papers prepared for publication.

III. EXPERIMENTAL PROCEDURES AND RESULTS

III.1. Recoil Test for Compressive Strength

Measurement of the compressive strength of single filaments of carbon fibers was performed using the recoil technique [3] In order to facilitate routine and reliable testing of different carbon fiber samples, an experimental rig, shown schematically in Fig. 1, was fabricated.

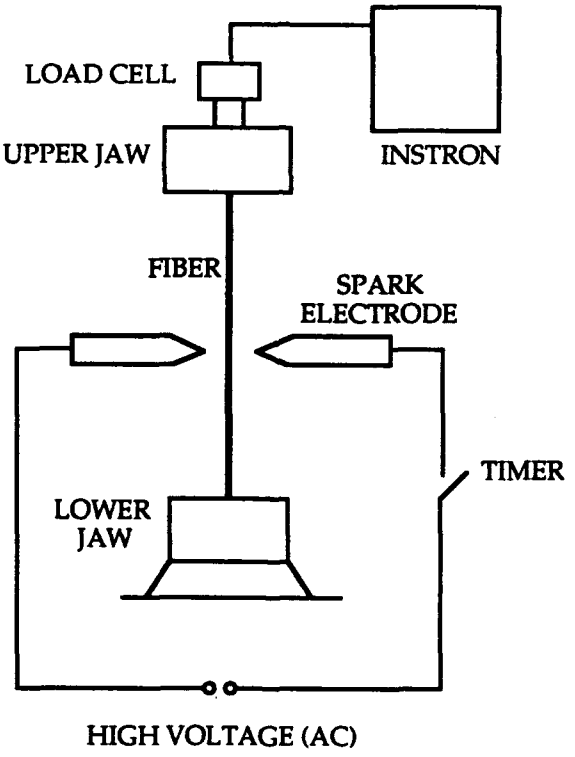

Fig. 1. Schematic of Recoil Test Apparatus.

A standard Instron 1125 instrument with a 500 g load cell was used. Since the fiber samples typically failed at forces less than 20 gf, the full scale range selected on the load cell amplifier was 20g. Apart from the usual electronic calibration, a crosscheck was also performed by hanging accurately known weights to the clamp.

The fiber specimen was glued onto a precut paper tab which allowed for a gauge length of 1 inch. In order to prevent blotting of the adhesive, a commercial non-drip, cyanoacrylate formulation was used. Any possible damage to the fiber from cutting the tab was reduced by cutting one side of the tab prior to sticking the fiber onto the tab.

A typical test for detection of a compressive failure involved the following procedure. The paper tab (with the specimen) was mounted carefully on the Instron tester. The top part was gripped using a spring loaded fiber clamp supplied by Instron. The tab was next gripped at the bottom using pneumatic clamps. Vertical mounting was checked visually. The tab was next separated by cutting the bridging paper segment using a pair of scissors. Any lack of care at this point would result in jarring which could break the mounted single filament sample. This proved to be the single most common cause of wastage of specimens. The fiber sample was next loaded to a predetermined tensile force using a digital multimeter to monitor the output of the stress transducer. A resolution of 0.01V yielded a corresponding force resolution of 0.01 gf. The crosshead speed utilized for this pretensing was initially 0.1 inch/min, with slower speeds of 0.02 and 0.005 inch/min used for fine control once a force level in the vicinity of the desired level was reached.

The cutting of the fiber in tension was performed using an electrical spark generated between two pointed metal electrodes. The spark was generated using a 10kV transformer powered from a 110V AC wall outlet. The spark gap was ≈ 5/8 inch. In order to remove any uncertainty involved in the spark duration, a timer was introduced in the power line to facilitate a 'power-on' time of 0.1 sec. (Subsequent testing seemed to indicate that spark times of 0.1 s and 0.5 sec gave the same results.) Since aligning the electrodes around the specimen was both time-consuming and tedious, a small mechanical stage, mounted on linear bearings that allowed smooth horizontal movement, was fabricated. By sliding the stage, the spark gap could be made to align around the fiber in tension. The registration obtained with this device was sufficiently precise for this test and helped cut down the test time significantly.

It should be noted that the method of cutting employed by Allen [3] was a sharp pair of scissors. This scheme was investigated prior to using an electric spark, which was used originally by Wang et al. [9]. As expected, a much larger variation in values was seen with manual cutting. The discrepancy between the compressive strength values obtained with manual vs. spark cutting was especially severe with higher modulus fibers. This could be due the significantly larger stresses developed in the high modulus material during the process of inadvertently deforming the fiber while cutting it manually.

The recoil method involves inspection of the fiber near the clamps after the cutting has been performed. With carbon fibers, a break is believed to occur when the stress built up during the recoil exceeds the compressive strength. Absence of the fiber segment between the tab and the cutting point therefore

represents a failure in compression. The occurrence of a break in one tab and a no-break in the other tab was recorded as a break and a no-break. Once a value in the vicinity of the compressive strength of the sample was reached, a break implied lowering the next test's tensile load by 0.2 gf, while a no-break implied raising the next test's load by 0.2 gf. (This has also been referred to as the "up-down" or "staircase" method.) The range from the maximum force level at which the samples almost never failed to the minimum at which they almost always failed was typically about 1 gf, but larger ranges of 1.5 to 2.5 gf have also been observed.

Since the actual diameter of the fiber was not measured on each test specimen, the stress value corresponding to each failure was not known. The range of force values, combined with the average diameter of the fibers, were used to estimate the average, the minimum and maximum values of the failure stress.

The method of data collection and analysis described above does not provide much meaningful statistics regarding the nature of recoil strength distribution and its possible relationship to the true axial compressive strength of fibers. More extensive measurements and statistical analysis were, therefore, performed with PAN-based carbon fibers produced through carbonization at 1000°C. Twenty to forty specimens were tested at each force level, separated by 0.5 gf in the case of 1 inch and 3 inch gauge length samples, and by 1 gf in the case of 0.5 inch gauge length samples. The results from a refined statistical procedure for analysis of these recoil test data that lends itself easily to the estimation of physically meaningful characteristic material parameters such as "zero gauge length" (ZGL) compressive strength are summarized in section III.4. Details of the tests and statistical modeling are given in appendix II.

III.2. Preparation of Fiber Samples

A broad range of samples have been sought for the proposed investigations regarding the evolution of compressive strength in the formation of carbon fibers. The motivation here has been to explore not only the evolutionary aspects in the conversion of current commercial precursors, but also the mechanisms by which different morphologies can be obtained in the carbon fibers. The following have been investigated in this regard.

(i) Role of Carbonization Temperature:

It is well known that the extent to which chemical and morphological transformations to a turbostratic graphite-like structure occurs (even with prolonged exposure) increases monotonically from the low end of carbonization temperatures (800°C) to the high graphitization temperatures (>2500°C). In order to explore these morphologies and the consequent mechanical properties, one set of experimental carbon fibers that had been processed at different temperatures have been obtained from an industrial laboratory. These fibers will be referred in this study as

terminal fibers.

(ii) Evolution within a Continuous Carbonization Process

We have shown earlier that the chemical and morphological changes occur at different rates in a carbonization process, with the former having to necessarily precede the latter in forming the carbonized structure [4]. Thus a carbonization process with a set maximum temperature is fully characterized in this regard only when the role of time-stress-temperature interactions are established. Carbonization, being a relatively slow process, lends itself well to such studies, i.e., it allows the generation of samples with increasing extent of transformation. This has been accomplished in the present study by (i) initially allowing continuous carbonization to reach a steady state, (ii) cutting the fiber at the exit of the furnace, and (iii) withdrawing the fiber rapidly from the inlet end. This length of fiber is cut into sections and the fibers within each section are characterized for their morphological features, chemical composition and mechanical properties. In order to ensure that a high quality of processing, fibers processed in the above described manner were also obtained from an industrial pilot research facility, with the fibers processed under conditions of a linearly increasing temperature profile (to the maximum temperature). Results from studies of these fibers are reported in section III.5.ii.

(iii) New PAN Precursor Fiber Morphologies

Alteration of the morphological features of PAN-based precursor fibers was sought by spinning a cosolution of PAN copolymer and a low concentration of PVA. The premise here was that the extent of development of lateral order in the fibers should be diminished by the need for excluding the "foreign" molecules (PVA) from the structure. Also, the nature of coagulation in fiber formation was expected to be significantly influenced by the much greater hydrophilicity of PVA. The solvent which is normally used for fiber spinning in our laboratories, DMF, was found to be unsuitable for this purpose because PVA precipitated out of the cosolution in DMF at room temperature. N-methyl pyrrolidone (NMP) was investigated for this purpose. Stable dopes of PAN/PVA in NMP were obtained with polymer concentrations up to 15%, with viscosities in the range suitable for fiber formation, namely, 100 to 1000 poise. Coagulation of extruded filaments was obtained in an NMP/water bath. *However, extensive experiments with this and other blends failed to yield new precursor fiber morphologies.* This approach to produce new carbon fiber morphologies was therefore abandoned.

(iv) Carbon Fiber Morphologies from Rod-like Polymer Precursors

In order to broaden the range of morphologies that can be obtained, formation of carbon fibers from liquid crystalline rod-like polymer fibers has been examined. These fibers provide an intermediate degree of order at the precursor stage, between the semi-rigid linear PAN and the mesophase plate-like pitch. Except for possible serendipitous observations, the purpose of this study was to create a new carbon fiber morphology and to study its mechanical behavior, especially in compression, so that the base of knowledge pertaining to 'morphology-properties' could be expanded. Results from this study are summarized in section III.3, with the details given in Appendix II.

III.3. Carbon Fiber Morphologies from PBZT Fibers

Conversion of poly(benzobisthiazole) – PBZT – fibers to carbon fibers has been studied in both batch and continuous processes. Themogravimetric analysis of PBZT fibers in nitrogen from room temperature to 1200°C revealed a significant weight loss in the range of 700-900°C. Thermal deformation analysis at low force levels, conducted by following the changes in the length of the fiber with a constant weight attached to its end, also revealed an apparent shrinkage (~10%) in the same temperature range. Pre-oxidation (up to 400°C), precarbonization (up to 850°C) and carbonization (up to 1600°C) have been carried out under tension to minimize shrinkage. An extensive series of experiments in this regard has revealed the following:

– Cohesively carbonized fibers can be obtained from PBZT fibers with a sequence of pre-carbonization (up to 850°C), followed by carbonization (up to 1600°C), with both processes being carried out in nitrogen and under a significant tension. A significant extent of the precursor orientational order is transferred to the carbon fibers, in spite of the cleavage that should have occurred at each monomer unit in the backbone from the loss of the heteroatoms. However, there is a diminution in orientation relative to the highly oriented precursor fiber that would cause a significant decrease in mechanical properties, especially because of the low inter-planar shear modulus of turbostratic carbon.

– Carbon fibers from PBZT fibers possess elongated microvoids (Fig. 2) as a consequence of the "dry-jet wet-spinning" process used to produce PBZT fibers and due to poor consolidation, both short-range and global. A natural consequence of the defects is a deterioration in mechanical properties. It is necessary to investigate if these properties could be improved by modifications that might improve consolidation of these carbon fibers and also reduce the diameters of, and defects in, the precursor fibers.

– PBZT-based carbon fibers exhibit a distinctly fibrillar morphology, with the fibrils finer than those in PAN-based carbon fibers (Fig. 3). The origin of these fibrils is clearly in the morphology of the precursor fibers. Interfibrillar microvoids and other defects such as surface striations can be seen in electron micrographs of PBZT-based carbon fibers (Fig. 4).

– Carbon fibers from PBZT fibers also often exhibit a well defined sheath-core morphology (Fig. 5) and also a skin on the sheath with a ribbon-like morphology (Fig. 6). It is not yet clear whether these arise from diffusion-dominated aspects of coagulation in precursor fiber formation or reaction at the carbonization stage. It should be noted that the size of the precursor fibers (~20 μ dia.) is much larger than that of typical high-performance carbon fiber precursors (~7μ dia.), thus making it susceptible to the formation of a sheath-core structure.

– PBZT fibers can be converted cohesively to carbon fibers. It offers a mechanism by which carbon fibers with different morphological parameters can be obtained. For example, the distinctly finer scale of fibril formation in the PBZT-based carbon fibers would allow examination of one of the mechanisms that has been proposed for failure in axial compression, namely, microfibrillar bucking. It is necessary, however, to eliminate the gross defects in the precursor fibers that are currently available before these can be used in studies of morphology–property relations in carbon fibers.

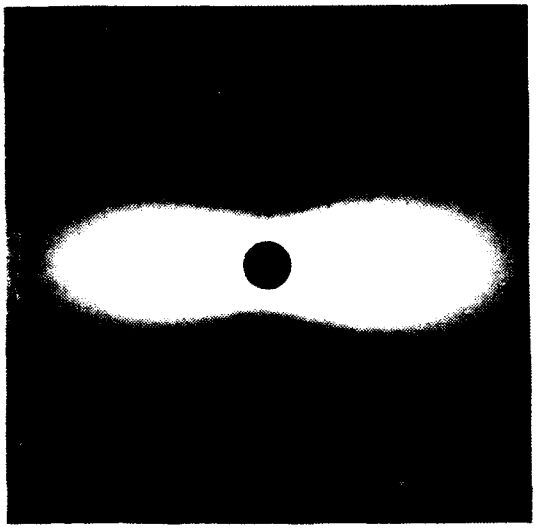

Fig. 2. SAXS pattern of PBZT-based carbon fibers from a continuous carbonization process at 1600°C indicative of elongated microvoids. Sample-to-film distance is 71.5 cm (Courtesy Gary Price, University of Dayton Research Institute).

(a)

(b)

Fig. 3. The fibrillar structure of PBZT-based carbon fibers: Processing temperatures – (a) 1200°C; (b) 1600°C.

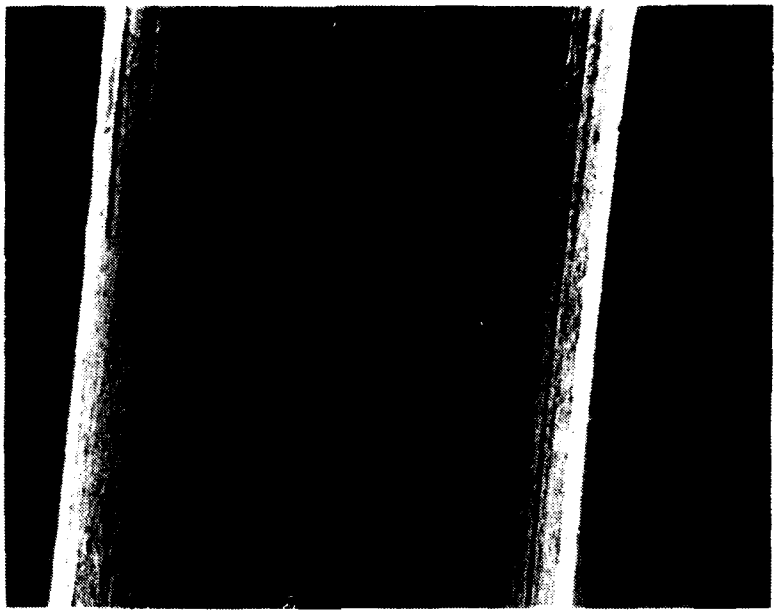

(a)

(b)

Fig. 4. SEM photographs, showing defects on the surface of PBZT-based carbon fibers: (a) longitudinal striations; (b) a large amount of microvoids formed between fibrils (Courtesy Gary Price, UDRI).

Fig. 5. SEM cross-section micrograph showing sheath-core structure in PBZT-based carbon fibers processed at 1600°C.

Fig. 6. The ribbon-like morphology composed of fibrillar structure in PBZT-based carbon fibers processed at 1600°C.

III.4. Statistical Model of Recoil Strength Distributions

The fibers employed for a detailed analysis of the tensile recoil test were produced at a carbonization temperature of 1000°C in an industrial laboratory (the complete series of fibers is described in the next section). Three different testing lengths (gauge lengths) of 0.5, 1.0 and 3.0 inches (12.7, 25.4 and 76.2 mm) were employed. The distribution of failure during the recoil process is shown in Fig. 7, expressed as the fraction of test specimens that failed during the recoil process when the fibers were cut at a specified tensile force. Two statistical models were employed for data analysis – Weibull and logistic. While both models could reasonably fit the available data, the latter was chosen as the more appropriate to fit the type of dichotomous data produced by the recoil test. The logistic model is given by

$$F(\sigma) = \frac{e^{\beta_0+\beta_1\sigma}}{1+e^{\beta_0+\beta_1\sigma}} \tag{1}$$

where σ is the applied recoil stress, $F(\sigma)$ is the model estimation of the fraction of fibers that fail under the applied stress, and β_0 and β_1 are model parameters (scale and stress parameters respectively). The model was extended into a "universal" model to include gauge length effects as follows

$$F(\sigma) = \frac{e^{\beta_0+\beta_1\sigma+\beta_2\sigma l+\beta_3 l}}{1+e^{\beta_0+\beta_1\sigma+\beta_2\sigma l+\beta_3 l}} \tag{2}$$

where $\{\beta_i\}$ are model parameters. A comparison of the individual and universal logistic distributions can be seen in Fig. 8, with the corresponding model parameters given in Table 1.

The average recoil strength, $\langle\sigma\rangle_r$, can be obtained from equation (2) and is given by

$$\langle\sigma\rangle_r = -\frac{\beta_0}{\beta_1+\beta_2 l} \tag{3}$$

An interesting limiting value of $\langle\sigma\rangle_r$ is its limiting value at zero gauge length, obtained as $l \to 0$. This value ($=-\beta_0/\beta_1$) can be viewed as an estimate of the true axial compressive strength. These and other aspects of the recoil strength distributions are discussed in detail in Appendix II. The most important results of this study are summarized in the following:

(1) The distribution of recoil strengths at a given test gauge length can be fitted well with Weibull as well as logistic distributions. However, a universal logistic distribution can provide a physically meaningful

framework for quantifying the distribution of recoil strengths as a function of gauge length.

(2) The experimentally observed decrease in recoil strength at longer gauge lengths should not be attributed to any "weak link"-based phenomenon, since failure in recoil occurs almost invariably in the zone close to the tabs to which the fiber is glued. The observed decrease is believed to be the consequence of higher bending stresses at longer gauge lengths. Support for this aspect is seen in regression analysis of "recoil from tension" (RFT) test data with a universal logistic distribution that reveals the predominant gauge length dependence to arise only through its interaction with the applied recoil stress.

(3) The universal logistic distribution with interactive gauge length–stress dependence allows a physically meaningful estimation of average recoil strength at zero gauge length (ZGL). Further research is necessary to determine if such an estimate corresponds to a ZGL estimate of true axial compressive strength.

(4) An overwhelming majority of RFT fracture surfaces of the PAN-based carbon fibers shows clearly a contribution from bending to failure. It is therefore inappropriate to consider the measured average recoil strength to be the axial compressive strength of these fibers at the corresponding gauge length. Nevertheless, the correlations observed experimentally to date [5, 7] and the possibility of estimating a ZGL recoil strength that eliminates bending-related terms represent good reasons for continued use and further exploration of this relatively simple method for estimating the potential performance of carbon fibers in axial compression.

Table 1. The Parameters of Universal Logistical Models

Statistical Model	Experimental Detail	Model Parameters			
		β_0	β_1 (GPa^{-1})	β_2 (GPacm)$^{-1}$	β_3 (cm^{-1})
Individual Logistic Model	Gauge Length				
	0.5 inch	-7.34	3.24	–	–
	1 inch	-10.02	4.86	–	–
	3 inch	-8.61	6.30	–	–
Universal Logistic Model	Failure Recorded at				
	Upper tab-end	-9.28	3.51	0.594	0.038
	Lower tab-end	-9.62	3.40	0.772	0.000
	Pooled upper & lower tab data	-9.62	3.42	0.690	0.000

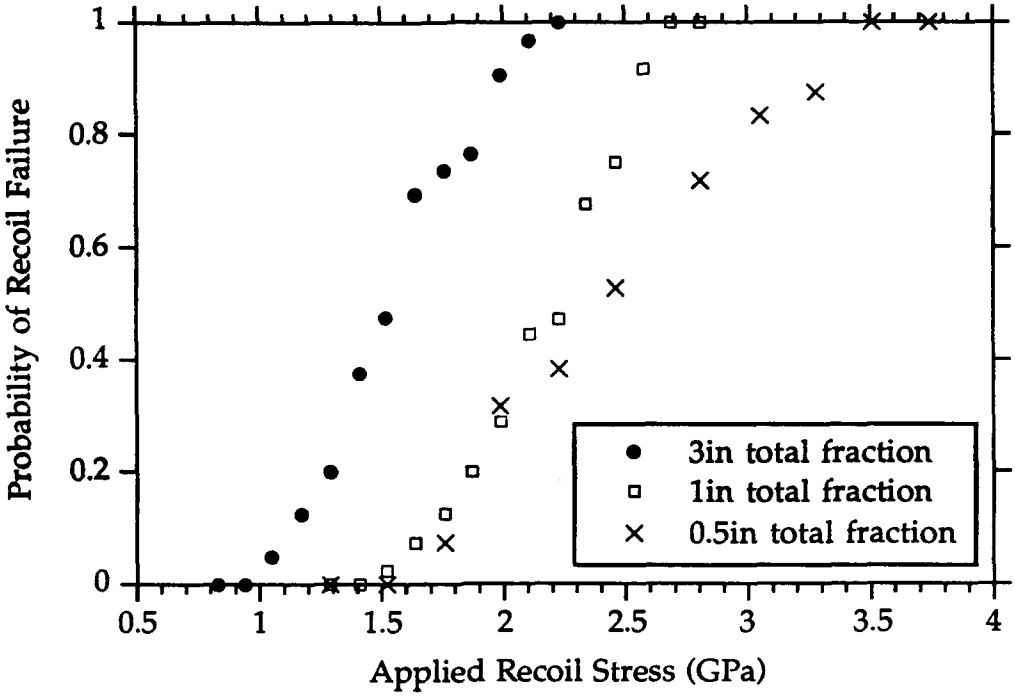

Fig. 7. Distribution of recoil failures at different gauge lengths for a PAN-based carbon fiber produced at 1000°C.

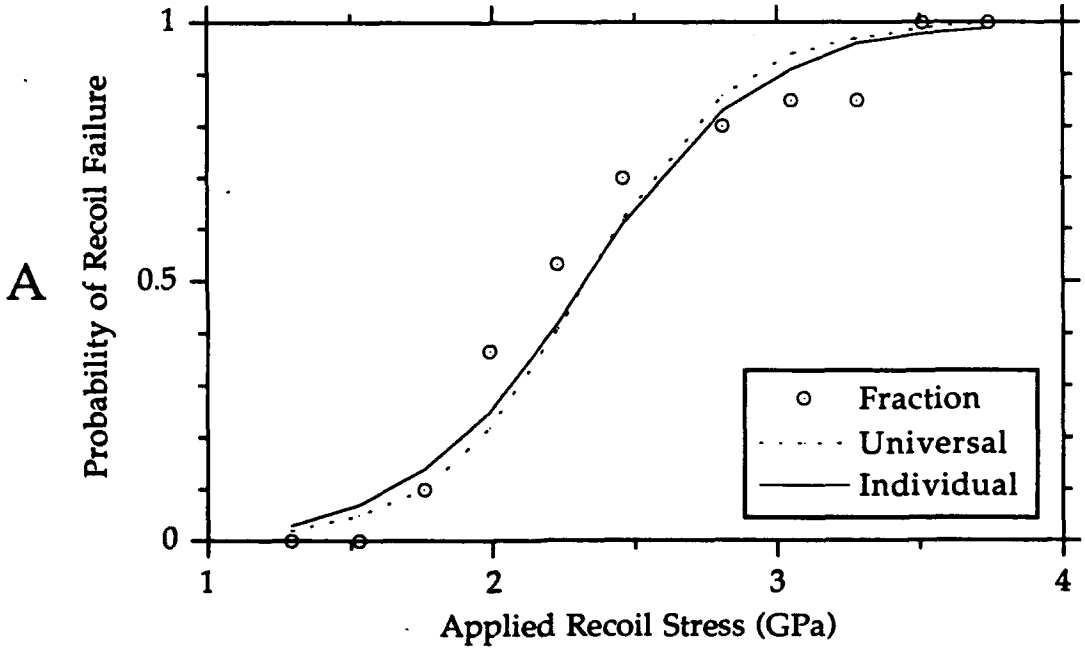

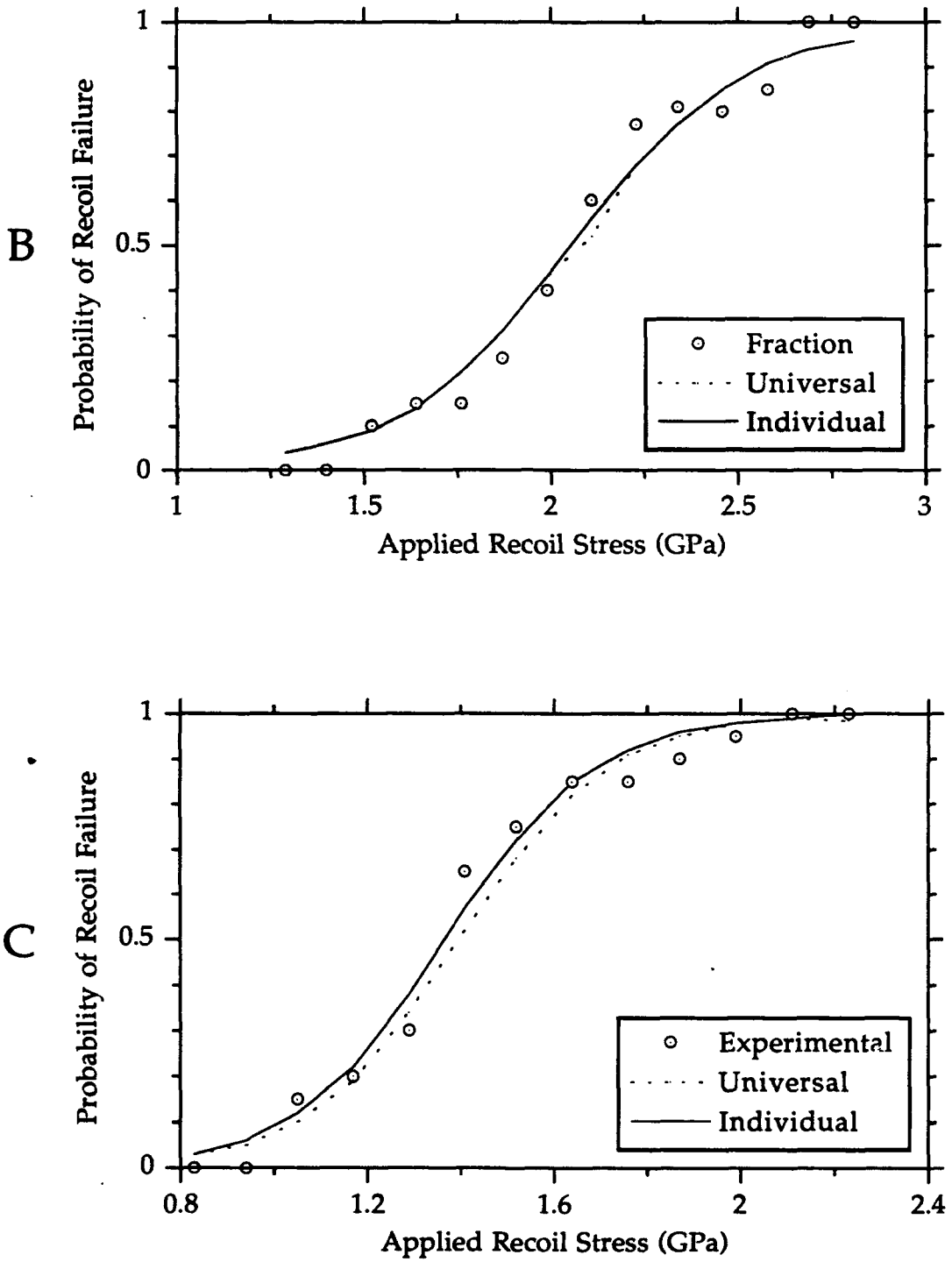

Fig. 8. Fits of individual and universal logistic distributions to recoil failure data for gauge length of (A) 0.5 in; (b) 1.0 in; and (C) 3.0 in. Model parameters for the distributions are given in Table 1.

III.5. Mechanical Properties

(i) Fibers Processed at Different Temperatures

The results from fibers which had been processed in an industrial laboratory are summarized in Table 2 and Fig. 9. It is appears that the evolution of mechanical properties in tension and in compression do not occur proportionately at different temperatures of carbonization. It also appears that compressive strength goes through a maximum at a lower temperature of carbonization than tensile strength.

The only aspect that appears to be significant here is that the evolution in compressive strength occurs in the temperature range corresponding to the formation of basal planes in the structure. It should be noted here that extensive crosslinking and aromatization of the structure would have preceded the formation of basal planes. Both tensile and compressive strengths diminish significantly in the low processing temperature range, up to 400°C, in which extensive ladder polymerization and crosslinking occur in the structure. The inference that might be drawn here with regard to high tensile performance organic fibers is that any hope for achieving a high compressive strength in them would rest on producing a more *laterally extensive primary* structure. Introducing a crosslinked network in a linear polymer, however dense, does not appear to be an appropriate path to achieving high compressive strength. If the evidence from the evolutionary path in the formation of PAN-based carbon fibers can be generalized, the inference would have to be that crosslinking might be detrimental to both tensile and compressive strength.

Table 2. Mechanical Properties of PAN-Based Carbon Fibers*

Processing Temperature (°C)	Tensile Strength (GPa)	Tensile Modulus (GPa)	Recoil Compressive Strength (GPa)	C/T ratio	Elongation %
270	0.33	1.9	C.S. ≈ T.S.	–	17.4
400	0.14	0.7	0.1	0.9	20
600	0.79	25	0.6	0.7	3.1
800	1.6	69	0.9	0.6	2.3
1000	2.6	143	1.9	0.7	1.8
1350	4.1	243	2.0	0.5	1.7
1700	4.4	310	1.8	0.4	1.4
2800	3.4	412	1.0	0.3	0.8

* Experimental fibers obtained from Courtaulds, U.K.

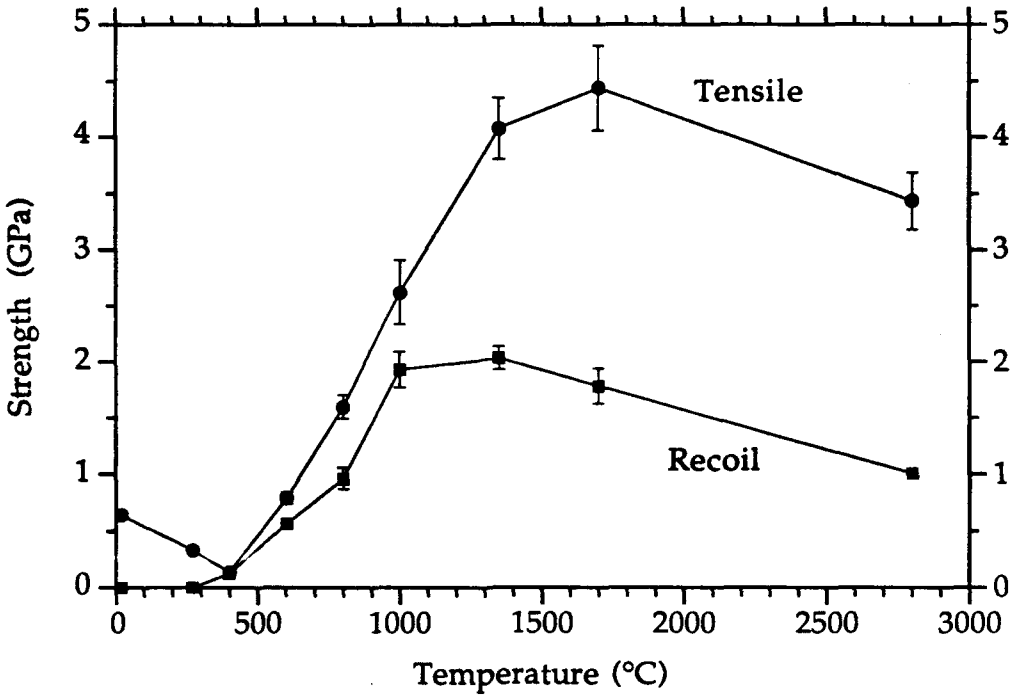

Fig. 9. Evolution of tensile and recoil compressive strengths of PAN-based carbon fibers as a function of carbonization temperature.

(ii) Evolution <u>within</u> Continuous Carbonization.

The conversion to carbonized structure and the evolution of fiber properties in continuous carbonization with the maximum furnace temperature of 1400°C are shown in Figs. 10–14. These "on-line" fibers were obtained in the manner described earlier in section III.2.ii. The results obtained from these experiments are similar to those with fibers obtained at the end of carbonization at different temperatures. Evolution in both tensile and compressive strengths require the development of the carbonized fiber morphology. The monotonic increase in the failure forces (Fig. 12) shows that a true increase in the load bearing capacity[1] occurs with the conversion of the crosslinked "stabilized" structure to the carbon fiber structure with its characteristic basal planes.

Strong positive correlations between torsional modulus and fiber compressive strength have been reported in the literature for a wide class of materials [6, 8]. It should be noted here that while much of the gain in torsional modulus occurs in

[1]Enhancement in failure stresses would be greater due to loss of material as well as densification of the structure.

the 800°C to 1000°C range (possibly caused by lateral couplings in the structure), there is a significant enhancement of recoil strength well beyond this range. It appears that enhancement in torsional stiffness is not the sole mechanism governing the evolution of recoil, or compressive, strength.

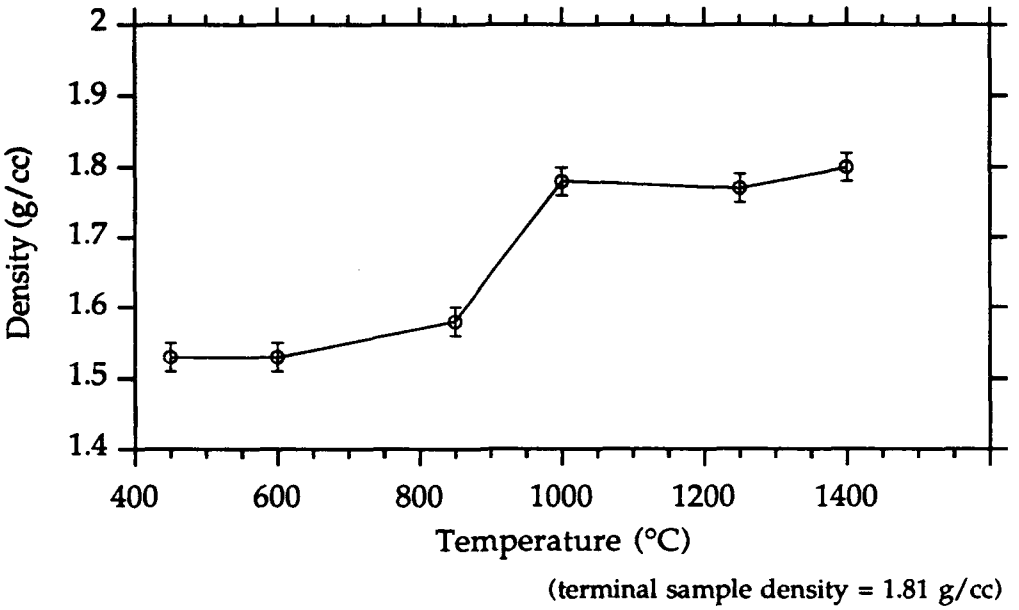

Fig. 10. Evolution of density in samples produced by continuous carbonization of a PAN-based carbon fiber at 1400°C.

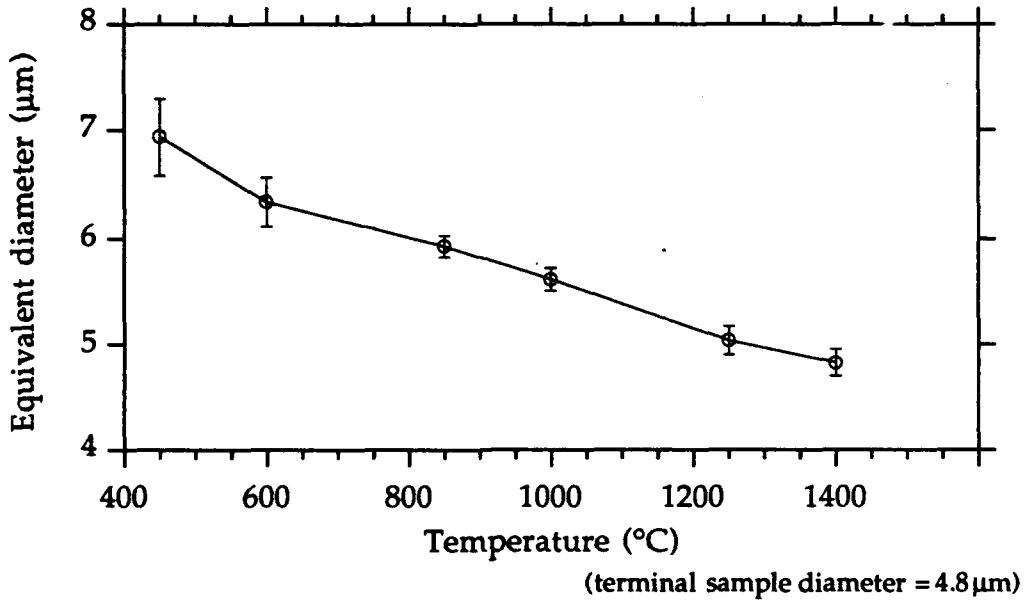

Fig. 11. Equivalent fiber diameters of carbon fibers carbonized at 1400°C.

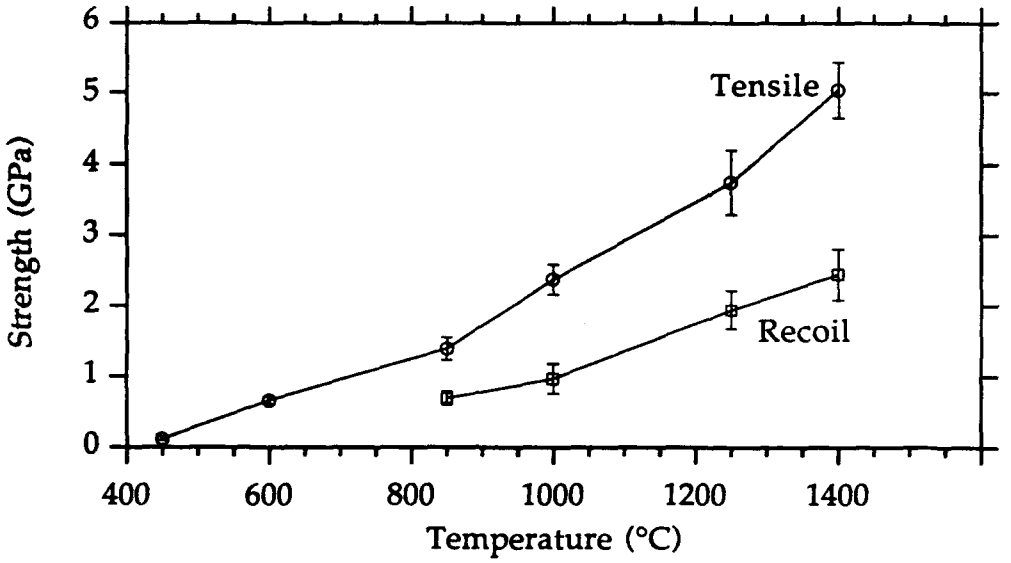

A

(terminal sample: tensile strength = 4.7 GPa
recoil strength = 2.5 GPa)

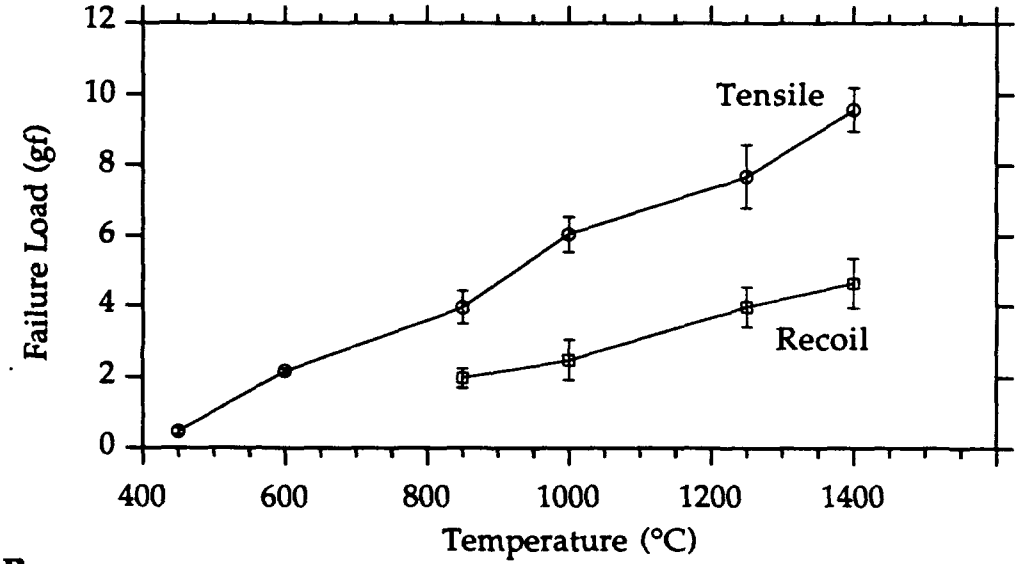

B

(terminal sample: tensile load = 8.6 gf
recoil load = 4.5 gf)

Fig. 12. Evolution of mechanical properties in samples produced by continuous carbonization of a PAN-based carbon fiber at 1400°C. (A) Tensile and Recoil strengths; (B) Failure loads. Gauge length = 1.0 inch.

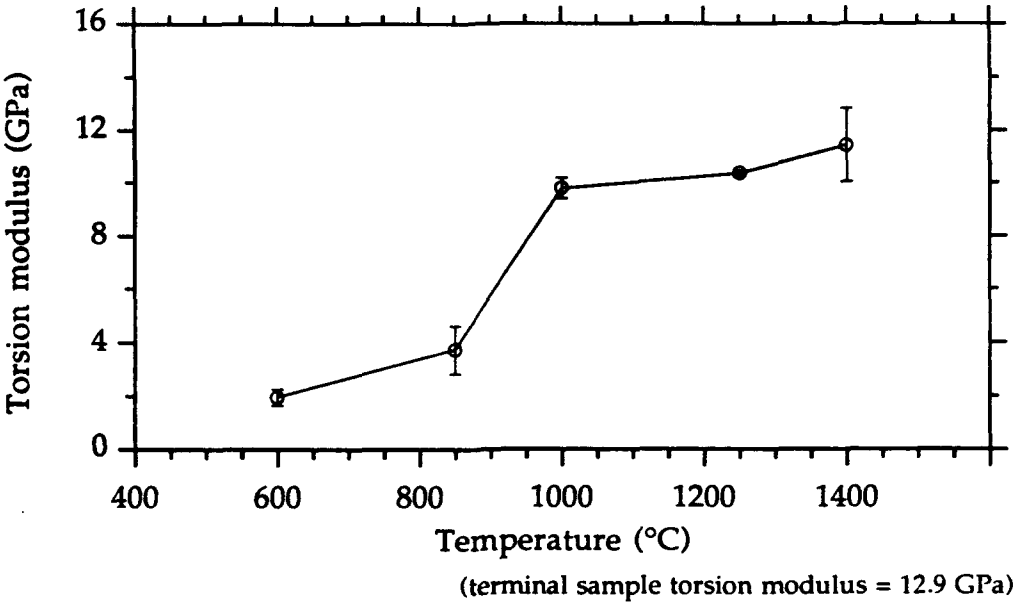

Fig. 13. Evolution of torsion modulus in samples produced by continuous carbonization of a PAN-based carbon fiber at 1400°C.

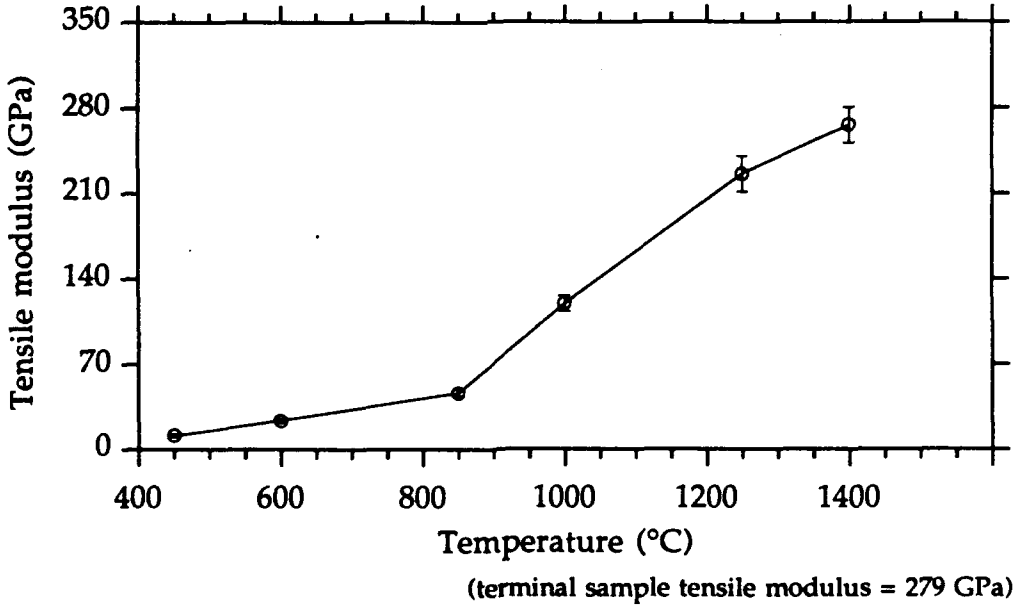

Fig. 14. Evolution of tensile modulus in samples produced by continuous carbonization of a PAN-based carbon fiber at 1400°C.

IV. CONCLUSIONS

The research reported here has produced important results pertaining to the measurement of axial compressive strength of high performance fibers and to the evolution of axial compressive properties in carbon fibers. The most important of these may be summarized as follows:

(a) The recoil test method, originally proposed by Allen [3], has been refined to reduce measurement-induced variations. Fracture surfaces of specimens from this experiment do not necessarily reveal failure in a simple compression mode and especially includes bending. A comprehensive atlas of fracture morphologies created during the recoil process has been compiled that show details of fracture initiation.

(b) Statistical analysis of the recoil method demonstrates that the fiber failure distribution can be expressed by either a logistic or a Weibull distribution. However, a universal logistic distribution of recoil failure stresses, containing an interactive stress–gauge length dependence, has been found to be physically meaningful and capable of fitting experimental data. It lends itself easily to the estimation of an average recoil strength at any gauge length and also to an extrapolated "zero gauge length" average. The latter is believed to represent a true "zero gauge length" average axial compressive strength of carbon fibers.

(c) Mechanical properties of fibers at different extents of progression toward the graphite fiber structure reveal that the evolutions of tensile and compressive properties are not synchronized. The results suggest that the degree of lateral correlation in the carbon fiber structure at which tensile strength reaches the maximum may be higher than that for maximum compressive strength. However, the differences in the observed patterns of evolution in tensile and axial compressive strengths are not large enough to warrant extensive further studies.

(d) Substantial enhancements in both tensile and compressive strengths of carbon fibers occur only with the development of the carbonized morphology with its characteristic basal planes as the fundamental structural units. While there is also a monotonic increase in torsional modulus in this region, the compressive strength (as measured by the recoil method) and the torsional modulus are not as strongly correlated as implied in previous literature.

(e) Studies aimed at generating different carbon fiber morphologies through the thermochemical conversion of precursors of rigid rod polymers show that PBZT fibers can be converted cohesively to carbon fibers. PBZT-based carbon fibers exhibit a distinctly fibrillar morphology, with the fibrils finer than those in PAN-based carbon fibers. A significant extent of the precursor orientational order is transferred to the carbon fibers, in spite of the cleavage that should have

occurred at each monomer unit in the backbone from the loss of the heteroatoms. It is necessary, however, to eliminate the gross defects in the precursor fibers that are currently available before these can be used advantageously in studies of morphology–mechanical property relations in carbon fibers.

(f) The implication from the carbon fiber studies for axial compressive strengths of high tensile performance organic fibers is that significant enhancement in this regard is not likely to result from merely crosslinking an oriented linear polymeric fiber. It does point, however, to the need for exploring possible "ordered crosslinking" of the structure, i.e., introducing regular crosslinks that enhance, or at least retain, the lateral order in these fibers.

V. REFERENCES

1. A. S. Abhiraman, "Fundamental Study of Compressive Strength Development in PAN-based Carbon Fibers," Annual Technical Report, submitted to Air Force Office of Scientific Research (1990).

2. A. S. Abhiraman, "Fundamental Study of Compressive Strength Development in PAN-based Carbon Fibers," Annual Technical Report, submitted to Air Force Office of Scientific Research (1991).

3. S. R. Allen, *J. Mater. Sci.*, **22**, 853 (1987).

4. M. Balasubramanian, M. K. Jain, S. Bhattacharya and A. S. Abhiraman, *J. Mater. Sci.*, **22**, 3864 (1987).

5. S. Damodaran, "Evolution of structure and mechanical properties during carbonization of PAN-based precursor fibers," Ph. D. Thesis, Georgia Tech., Atlanta, GA, (Nov. 1991).

6. S. J. DeTeresa, R. S. Porter and R. J. Farris, *J. Mater. Sci.*, **23**, 1886 (1988).

7. H. Jiang, S. Damodaran, P. Desai, S. Kumar, and A. S. Abhiraman, "Analysis of Tensile Recoil Method for the Compressive Strength Measurement of PAN-based Carbon Fibers", *Polym. Mater. Sci. Eng.*, **64**, 383 (1991)

8. T. Norita, A. Kitano and N. Noguchi, *Proc. of US-Japan Bilateral Conf. on Composite Materials*, June 27-29, 1988, p-548.

9. C. S. Wang, S. J. Bai and B. P. Rice, *Polymer Preprints*, **61**, 550 (1989).

APPENDIX I.
PAPERS AND PRESENTATIONS RESULTING FROM:

"FUNDAMENTAL STUDY OF COMPRESSIVE STRENGTH DEVELOPMENT IN PAN-BASED CARBON FIBERS"

(i) "New Aspects in the Conversion of Acrylic Precursors to High Performance Carbon Fibers," G. Bhat, S. Damodaran, P. Desai, L. H. Peebles, Jr., A. S. Abhiraman, AIChE Annual Meeting, San Francisco, CA, Nov. 6-9, 1989.

(ii) "Evolution of Compressive Strength during Carbonization of PAN-Based Fibers," S. Damodaran, Fall Technical Meeting of The Fiber Society, Nov. 1-3, 1989, Raleigh, NC.

(iii) "Evolution of Compressive Strength in PAN-Based Carbon Fibers," S. Damodaran, Southeastern Graduate Polymer Conference, Knoxville, TN, March 19-20, 1990.

(iv) "New Aspects in the Formation and Properties of PAN-based Carbon Fibers," G. Bhat, S. Damodaran, P. Desai, L. H. Peebles, Jr., A. S. Abhiraman, Symposium of Polymer Processing Society, Nice, France, April, 1990.

(v) "Carbon Fibers from Poly(p-Phenylene Benzobisthiazole) (PBZT) Fibers: Conversion and Morphological Aspects", H. Jiang, P. Desai, S. Kumar and A. S. Abhiraman, *Carbon*, **29**, 635 (1991).

(vi) "Analysis of Tensile Recoil Method for the Compressive Strength Measurement of PAN-based Carbon Fibers", H. Jiang, S. Damodaran, P. Desai, S. Kumar, A. S. Abhiraman and K. Tsui, PMSE Proceedings, vol. **64**, pp. 383-384, ACS Spring Meeting, Atlanta, GA, April 14-19, 1991.

(vii) "Analysis of Failure in Recoil from Tension of PAN-based Carbon Fibers", H. Jiang, A. S. Abhiraman and K. Tsui, manuscript submitted to *Carbon*.

APPENDIX II.
REPRINTS & PREPRINTS OF PAPERS RESULTING FROM:

"FUNDAMENTAL STUDY OF COMPRESSIVE STRENGTH DEVELOPMENT IN PAN-BASED CARBON FIBERS"

Carbon Vol. 29, Nos. 4/5, pp. 635–644, 1991
Printed in Great Britain.

0008-6223/91 $3.00 + .00

CARBON FIBERS FROM POLY (*p*-PHENYLENE BENZOBISTHIAZOLE) (PBZT) FIBERS: CONVERSION AND MORPHOLOGICAL ASPECTS

H. JIANG, P. DESAI, S. KUMAR and A. S. ABHIRAMAN[1]
Polymer Education and Research Center, Georgia Institute of Technology, Atlanta, GA 30332, U.S.A.

(*Received* 17 *September* 1990; *accepted in revised form* 14 *November* 1990)

Abstract—Conversion of highly oriented stiff-chain Poly (*p*-phenylene benzobisthiazole) (PBZT) fibers to carbon fibers was investigated in both batch and continuous processes. The PBZT-based carbon fiber shows a structure somewhat different from those of conventional carbon fibers, with well-defined fibrils and micro-fibrils oriented along the fiber direction. There exists also a sheath-core structure. The fiber surface shows a large amount of microvoids. These morphological features appear to be directly related to features in the precursor fibers. The prospects for producing useful new carbon fiber morphologies from these precursors are discussed.

Key Words—Carbon fibers, PBZT fibers, carbonization.

1. INTRODUCTION

Since the formation of carbon fibers from cellulose-based fibers in the last century, it has been well known that carbon fibers could be produced through controlled pyrolysis of several carbon-containing precursor materials[1]. Progress in this field has been especially rapid in the last three decades. The precursors in current production are comprised predominantly of poly(acrylonitrile) (PAN)[2–4] and aromatic pitch materials[2–4]. Mechanical properties superior to those of most other materials have been achieved, especially in tension. Carbon fibers with modulus and tenacity in excess of 800 GPa and 3 GPa, respectively, have been obtained.

Recent progress notwithstanding, there is still considerable interest in research on carbon fiber formation, motivated by the desire to reduce their cost or the need to improve mechanical performance. Use of these fibers is still limited by their less-than-desirable performance in compression. Advances along these lines have been limited by the inability so far to produce a broad range of morphologies with which a base of morphology-property relations can be established for these fibers. Current research in our laboratories towards this end is based on either modification of the morphologies of PAN-based precursor fibers or by using other precursors for conversion to carbon fibers.

Formation of carbon fibers from a class of relatively rigid polymers, aromatic polyamides, has been investigated by Ezekiel and Spain[5,6], and Tomizuka *et al.*[7,8]. These exploratory studies revealed that elements of the morphology of precursor fibers were indeed retained through the process of conversion to carbon fibers, but quantification of chemical and morphological evolution was lacking in these studies. We report here the results from ongoing research in our laboratories to generate new carbon fiber morphologies with a rigid-rod precursor polymer. Fibers of poly(*p*-phenylene benzobisthiazole) (PBZT), a linear stiff chain polymer (Fig. 1), were chosen for this purpose. Although their mechanical properties in tension are comparable to those of good carbon fibers, the compressive strength of PBZT fibers is only a tenth of the tensile strength[9]. Their morphology is significantly different from that of PAN-based fibers[2–4,10–15]. These fibers offer, therefore, the prospect of yielding new carbon fiber morphologies.

2. EXPERIMENTAL

2.1 *Precursor fibers*

The PBZT fibers used in this study were supplied by the Material Research Laboratory, Wright Patterson Air Force Base. Data pertaining to the fiber properties are given in Table 1. The molecular weight of the polymer is about 25,000. The fibers had been spun from a nematic solution with the dry-jet wet spinning technique. Then the as-spun fibers were dried and heat treated (HT) under tension at about 650°C to achieve superior mechanical properties. The yarn tow contained approximately 290 filaments, with a denier of 949. They have a circular cross-section and their morphology is comprised of fibrils (shown in Fig. 2). It has been reported that the fibrils are made up of linear extended molecular chains that align nearly along the fiber axis direction[15,16]. Figure 3 shows the wide angle X-ray and small angle X-ray scattering (WAXS and SAXS) patterns for the HT PBZT fibers. The WAXS pattern in Fig. 3A,

[1]To whom correspondence should be addressed

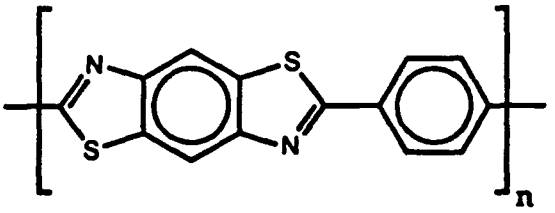

Fig. 1. The structure of PBZT.

with the 100 and 010 reflection on the equator and no off-equatorial reflections except for the layer lines, is consistent with the highly oriented two-dimensionally ordered crystal structure that has been reported for the PBZT fibers[15,16]. Figure 3B exhibits a diffuse, continuous distribution of intensities in SAXS along the equator implying the existence of microvoids elongated along the fiber direction in the PBZT fibers.

2.2 *Conversion to carbon fibers*

The initial experiments were conducted in the batch process mode, primarily to establish the feasibility of conversion of PBZT fibers cohesively to carbon fibers and to perform a preliminary investigation of the morphological features and mechanical properties of the product. The PBZT filament bundle was mounted in a horizontal Lindberg furnace that was purged continuously with a stream of N_2 gas; a static tensile force of 10–200 g was applied to the filament bundle. The temperature of the furnace (initially room temperature) was raised to 850°C over a period of about 60 minutes, maintained at this temperature for 10 minutes, and raised further to either 1200° or 1600°C in about 60 minutes. In another set of experiments, the precursor fibers were subjected to pre-oxidation overnight in the air at 390°C before the carbonization as described above.

Continuous conversion to carbon fibers was also carried out with and without pre-oxidation. In the process with pre-oxidation, the PBZT fiber tow was passed through three ovens. The first oven, for pre-oxidation, was a three-foot long Lindberg furnace at 450°C in air. The second was a 1.5-foot long heater at 850°C in N_2 environment and the third was another three-foot Lindberg furnace at 1200° or 1600°C purged with N_2 flow. The filament feed rate was about 2 feet/min, and the tension on the sample, controlled in the range from 10 to 200 g, was monitored by means of an in-line force transducer. For the treatment without pre-oxidation, only the first and third ovens were used, both under N_2. The maximum temperatures in the two furnaces were, respectively, 850° and either 1200 or 1600°C. Typical temperature profiles in these furnaces are shown in Fig. 4.

2.3 *Thermogravimetric analysis (TGA)*

The PBZT fiber was cut into small pieces and thermogravimetric analysis conducted using a Perkin Elmer TGA-7 in N_2 flow up to 1200 and 1400°C with heating rates of 20°/min and 10°/min, respectively.

2.4 *X-ray scattering (WAXS and SAXS)*

By means of a Rigaku Rotaflex RU-200B rotating anode X-ray generator, both WAXS and SAXS photographs were taken with a flat film camera in an evacuated chamber. The operating voltage was 45kV and current 100 mA. Ni filtered Cu—Kα radiation was used and the pinhole size was 0.5 mm. The distances between the sample and the film (SFD) were 3.5 cm and 29.5 cm for WAXS and SAXS, respectively.

2.5 *Scanning electron microscopy (SEM)*

All specimens were sputter-coated with a thin layer of Au—Pd alloy and observed in a Cambridge Stereoscan 90 SEM operating at 15kV. (Fig. 14 is from Hitachi S-900).

2.6 *Density measurements*

Two techniques were used to measure the density of carbon fibers. One was the flotation method. Liquid mixtures of tetrabromoethane ($Br_2CHCHBr_2$) and CCl_4 were used to determine the density. First a liquid mixture of density lower than the sample density was prepared. Then a small bundle of the fiber sample was immersed in the mixture. This was done to confirm that the specimen sank and did not have trapped air bubbles. Next, small volumes of $Br_2CHCHBr_2$ were successively added and the mixture shaken well to homogenize the density and allowed to rest until the specimen just floated in the bulk of the fluid after 20 minutes. Next, the density of the fluid was measured with a Calculating Digital Density Meter (PAAR/DMA-45).

The other technique employed was Helium Multipycnometry using a Quantachrome Helium Pycnometer (Model MVP-1) by measuring the volume of a known mass of finely-cut carbon fibers.

2.7 *Mechanical properties*

2.7.1 *Single filament tensile tests.* The fiber specimens were mounted on thin cardboard tabs at a gauge length of 1 inch by using a quick-gel glue. Samples were extended to failure on an Instron (Model 1125) at a rate of 0.05 in/min (5%/min)

Table 1. Properties of HT PBZT fiber[16]

Material	Young's modulus	Tensile strength	Elongation to break	Compressive Strength	Density g/cm³	Diameter μm
HT PBZT Fiber	300 GPa	4.2 GPa	1.3%	400 MPa	1.58	20.0

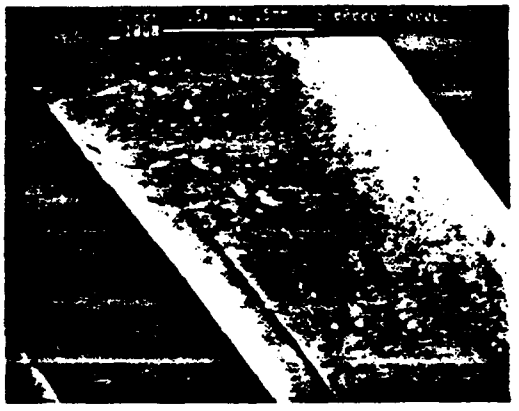

(a)

(b)

Fig. 2. SEM micrographs of (A) surface morphology of HT PBZT precursor fiber: (B) axial spliting and fibril structure of fractured HT PBZT fiber.

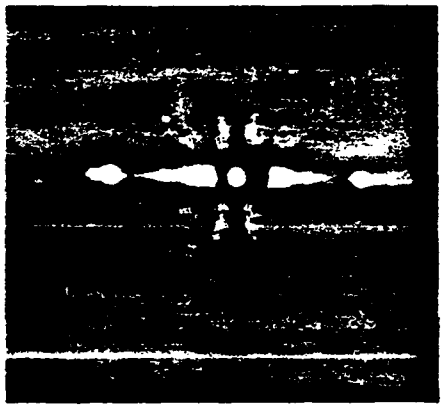

(a)

(b)

Fig. 3. (A) WAXS pattern of HT PBZT fibers showing the distinct scattering spots of (100) and (010) crystalline planes along the equator: (B) SAXS photograph of HT PBZT fibers showing a diffuse, continuous equatorial scattering.

using a 500 g load-cell to measure forces. Tensile modulus was evaluated from the tensile stress-strain curve and compliance correction was not made because of the limited specimen. Therefore the value without compliance correction would be lower than the true modulus. The cross section of the sample was assumed to be perfectly circular and the average diameter was obtained from measurements on SEM photographs.

2.7.2 *Single filament recoil compressive tests.* The recoil method, proposed originally by Allen[14], was adopted for compressive strength measurements. The fiber samples were stretched in the Instron to a desired tensile stress level, and then cut by an electric spark at the center of the gauge length (1 inch)[17]. Both halves of the tabs with the remaining fibers were carefully collected from the clamps for examination. Each portion was examined, thus providing two results per test sample, to ascertain whether or not fracture occurred due to the compressive forces that develop in recoil. The compressive strength was calculated as the average of two extreme values (i.e.,

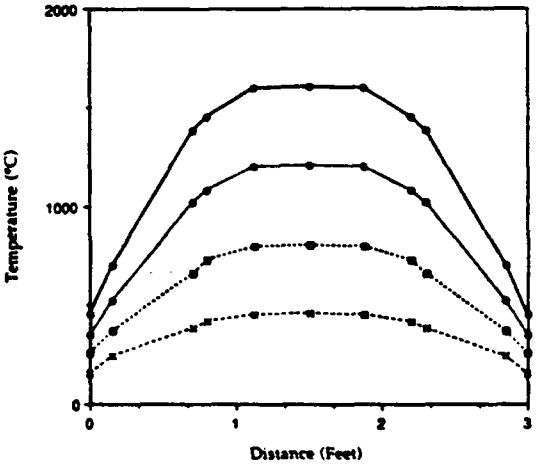

Fig. 4. Temperature profiles in the carbonization furnace.

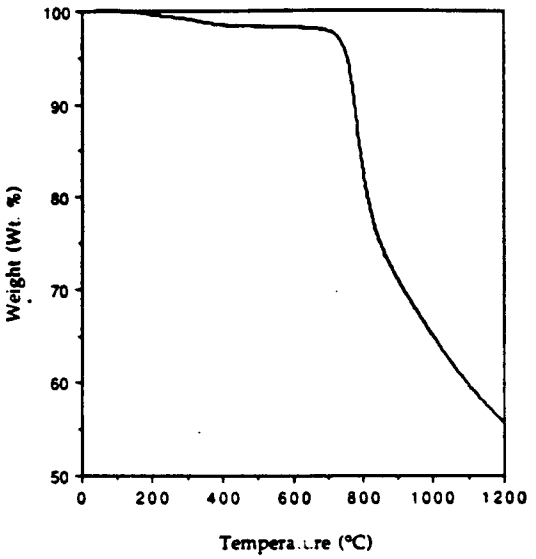

Fig. 5. Thermogram of HT PBZT precursor fibers from 20°C to 1200°C obtained at a scanning rate of 20°C min under N_2 atmosphere. Rapid loss of weight begins at about 700°C. Residual weight at 1200°C is about 55% of the original material.

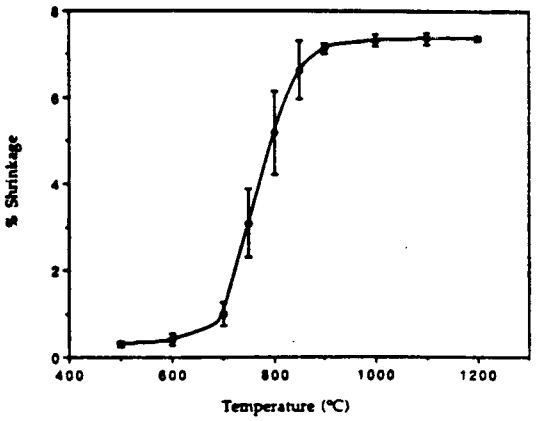

Fig. 6. Logitudinal shrinkage (%) of PBZT fibers with process temperature. The temperature range in which shrinkage occurs coincides with that of rapid weight loss in the thermogravimetric analysis. Shrinkage is negligible above 900°C.

the maximum force at which both end-tabs always remained unbroken and the minimum force at which both or one of the two end-tabs were always broken). Five filaments were tested at each imposed force level.

3. RESULTS AND DISCUSSION

3.1 *Batch processing*

Thermogravimetric analysis (TGA) of the precursor was carried out in order to infer the appropriate conditions for converting it to carbon fiber. Figure 5 shows the thermogram obtained in a nitrogen environment for the PBZT fibers. A rapid weight loss occurs at temperatures above 700°C. The yield at 1200°C is approximately 55% of the starting material. The theoretical yield for carbon from PBZT, assuming loss of all but carbon, is 63%. The theoretical yield of carbon assuming that carbon in the benzobisthiazole moiety is also lost is 54%. The results from elemental analysis are given in Table 2. At 850°C, most of the hydrogen is lost and above 1200°C, there is hardly any hydrogen in the carbon fibers. Approximately 80% of the nitrogen and sulfur are removed when the temperature is raised to 1200°C. The structure still retains about 5% of these elements after processing at 1600°C. It is interesting to note that the N/S ratio remains essentially the same as in the original PBZT structure, implying cooperative loss of these elements in the thiazole moiety. The change in concentration of carbon atoms indicates that the carbon in the thiazole moiety is lost along with nitrogen and sulfur. The change in N/S ratio reported at 1600°C is probably the result of errors in measurement at the low concentrations of these elements retained at this temperature.

Associated with the reactions which lead to loss of non-carbon elements is a shrinkage in the length of fibers (Fig. 6). The cumulative longitudinal shrinkage that occurs in the 700–900°C range is around 9%. Little change is observed at temperatures below or beyond this range. The temperature at which the onset of shrinkage occurs in the preoxidized material is only slightly higher than that for the non-oxidized precursor. This shrinkage is believed to arise from loss of elements of polymer backbone and the decrease in length associated with the formation of the carbon bonding sequence. The lat-

Table 2. The results of elemental analysis of PBZT-based carbon fibers

Material	Contents (%)C	(%)N	(%)S	(%)H	N/S Ratio
HT PBZT Fiber*	63.2	10.5	24.1	2.3	0.44
PBZT CF (850°C)	76.3	6.9	15.7	0.3	0.44
PBZT CF (1200°C)	91.2	2.2	5.1	—	0.43
PBZT CF (1600°C)	98.6	0.6	2.1	—	0.27

*Estimated from the PBZT repeat unit.

Table 3. Properties of PAN- and PBZT-based carbon fibers

Carbon Fibers	Processing Temperature (°C)	Diameter (μm)	Density (immersion) (g/cm³)	Density (pycnometry) (g/cm³)	Tensile Strength (GPa)	Tensile* Modulus (GPa)	Compressive Strength (GPa)	Elongation to break (%)
Pan-	800	7.7	1.769	1.850	1.77	69	0.96	2.3
based	1350	7.0	1.797	1.877	3.90	243	2.03	1.7
	1700	6.6	1.798	1.891	4.00	310	1.78	1.4
PBZT-	850	18.5	1.592	1.697	0.33	56	0.20	0.6
based	1200	16.0	1.684	1.843	0.50	136	0.37	0.6
npo**	1600	15.3	1.716	1.856	0.76	137	0.43	0.6
PBZT-	850	19.2	1.592	—	0.36	54	0.20	0.6
based	1200	15.9	1.684	—	0.82	137	0.41	0.6
po***	1600	14.8	1.716	—	0.93	196	0.65	0.5

*Without compliance correction.
**Not pre-oxidized.
***Pre-oxidized.

eral dimension also begins to decrease around 700°C due to material loss and consolidation of the structure. It continues well beyond the range of primary material loss because densification of the structure increases monotonically with temperature.

It should be noted here, however, that the densities obtained with the immersion-flotation method would be affected significantly by dilatation caused by microvoids in the fibers (Table 3). Most of the microvoids in such fibers are usually inaccessible to the fluid medium in this simple immersion method. This aspect of fiber morphology is discussed further in the context of continuously processed fibers (see section 3.2).

Other morphology-related investigations with batch-processed fibers revealed clearly that an oriented carbon fiber structure indeed resulted from conversion of the PBZT fibers (see, for example, the WAXS patterns from fibers processed at 1200 and 1600°C shown in Fig. 7). A significant extent of the precursor orientational order is thus transferred to the carbon fibers, in spite of the cleavage that should have occured at each monomer unit in the backbone from the loss of hetero-atoms.

3.2 *Continuous processing*

The conditions for continuous conversion to carbon fibers always included thermal treatment at 850°C, which is in the range where the major reactions for the elimination of non-carbon elements take place (Fig. 5). This was done primarily to control carbonization reactions before carrying out further consolidation at temperatures of 1200 and 1600°C.

Flat-plate WAXS patterns obtained from fibers that had been produced at different temperatures are shown in Fig. 8. With fibers that had been processed below 450°C, the diffraction pattern is nearly the same as that of the precursor PBZT fibers. The diffraction patterns after processing at 850, 1200 and 1600°C are typical of those of carbon fibers from other precursors, such as PAN. The distinct (002) diffraction that is concentrated around the equator and the faint (101) diffraction close to the meridian

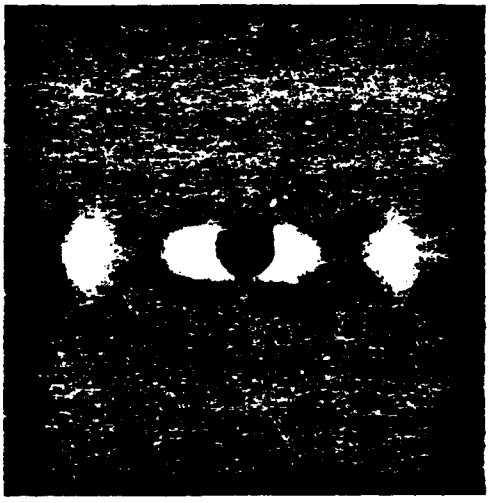

(a)

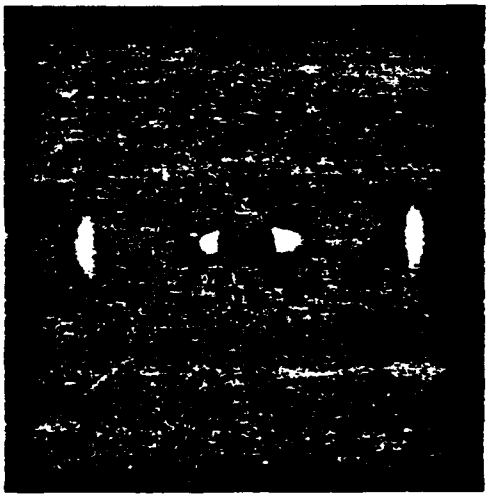

(b)

Fig. 7. WAXS patterns of PBZT-based carbon fibers from a batch process, (A) at 1200°C; (B) at 1600°C.

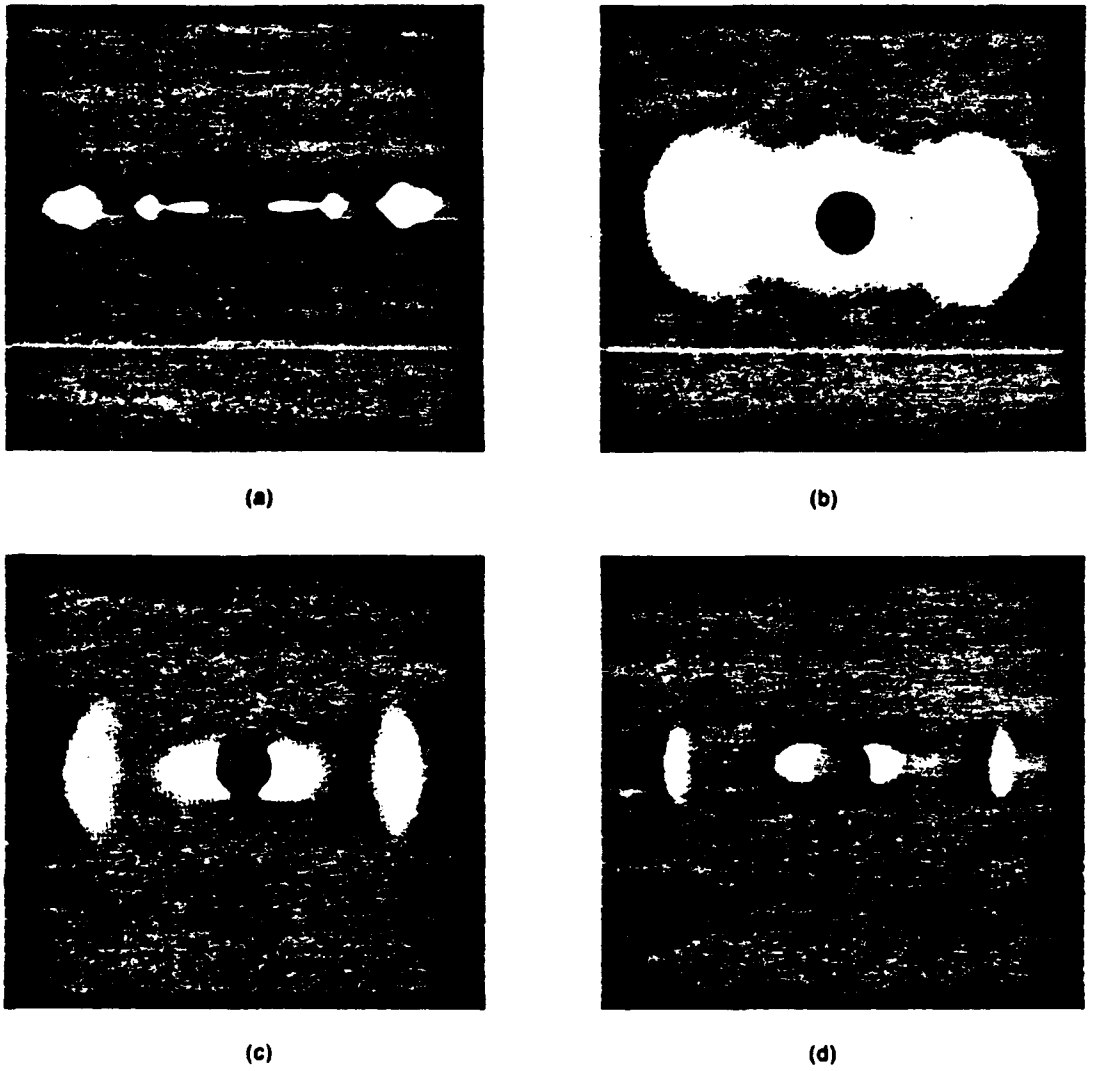

Fig. 8. WAXS patterns of (A) the PBZT precursor fibers treated overnight at 390°C in air. It looks similar to Fig. 4, a WAXS pattern of the original precursor; (B) PBZT-based carbon fibers from a continuous process at 850°C; (C) PBZT-based carbon fibers from a continuous process at 1200°C; (D) PBZT-based carbon fibers from a continuous process at 1600°C.

Table 4. Morphological parameters from WAXS of PAN- and PBZT-based carbon fibers

Carbon Fibers	Processing Temperature (°C)	Azimuthal Scan Half-width (002) (°)(ϕ)	Equatorial Scan Half-width (002) (°)(2θ)
PAN-based CF	800	42	3.2
	1350	36	2.3
	1700	30	1.7
PBZT-based CF*	850	43	4.0
	1200	39	2.8
	1600	34	1.9

*Without pre-oxidation; continuously processed.

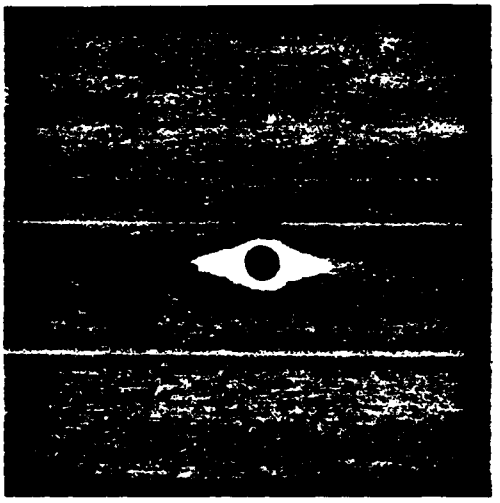

(a)

(b)

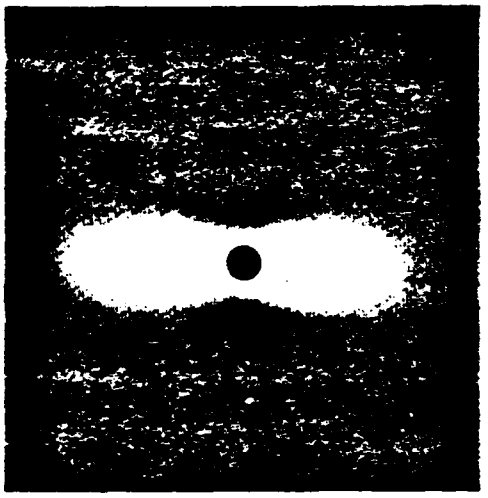

(c)

Fig. 9. SAXS patterns of PBZT-based carbon fibers from a continuous process: (A) 850°C; (B) 1200°C; (C) 1600°C. (photographs obtained by Gary Price, University of Dayton Reseach Institute, with SFD of 71.5 cm).

are clearly associated with the development of a crystal structure with "basal planes" oriented along the fiber axis. This aspect of the evolution of carbon fiber structure is most essential for the development of tensile strength and modulus. The half-width in the azimuthal scan of the (002) reflection (Table 4) is, however, significantly higher than that of the (010) reflection in the precursor PBZT fibers. This diminution in orientation would cause a significant deterioration in mechanical properties, especially because of the low inter-planar shear modulus of turbostratic carbon.

The equatorial scattering intensity in SAXS increases with processing temperature (Fig. 9) indicating a higher concentration of elongated microvoids in the fibers treated at higher temperatures. Although such microvoids are well known to be present in oriented carbon fibers from all precursors, the indication from these PBZT-based fibers is that their concentration and size are significantly higher. The origin of a fraction of these microvoids is in the precursor fiber, a consequence of its "dry-jet-wet" spinning process. It is also clear that a substantial amount of these are newly formed during carbonization through the combination of material loss and localised, rather than global, densification. This aspect is also seen clearly in the density and diameter data given in Table 3. For both PAN- and PBZT-based carbon fibers, the densities obtained by the floatation method are much less than those obtained with the pycnometer. It is apparently due to greater accessibility of the microvoids to the high pressure He gas. However, the densities of the PBZT-based carbon fibers are still lower than those of the PAN-based fibers which had been processed at corresponding temperatures.

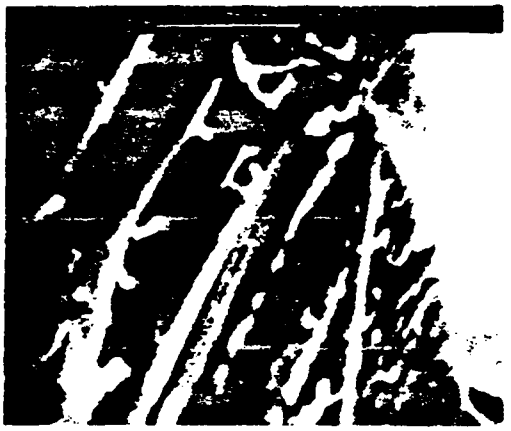

(a)

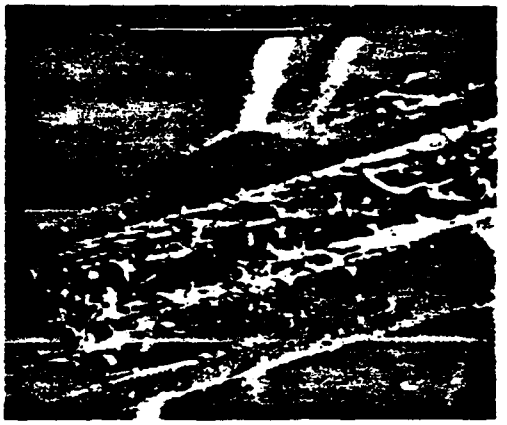

(b)

(c)

Fig. 10. The fibrillar structure of PBZT-based carbon fibers: Processing temperatures - (A) 850°C; (B) 1200°C; (C) 1600°C.

It is possible that the "misoriented" fraction, in the PBZT-based carbon fibers is a consequence of poor consolidation, both short-range and global. The half-widths obtained from both the equatorial and the azimuthal scans of the (002) reflection with PBZT-based carbon fibers are higher than those of PAN-based fibers (Table 4). Higher concentrations of microvoids would also lead to a correspondingly higher concentration of misoriented domains around them.

A natural consequence of the defect features that have been observed in the PBZT-based carbon fibers is deterioration in their mechanical properties. Tensile strength, tensile modulus, and elongation at break are significantly lower than the corresponding properties of the precursor and other carbon fibers (Tables 1 and 3). Pre-oxidation prior to carbonization appears to provide an improved conversion, although it is still far from reaching desirable properties. It is necessary to investigate if these properties could be improved by modifications that might improve consolidation of these carbon fibers and also reduce the defects in the precursor fiber.

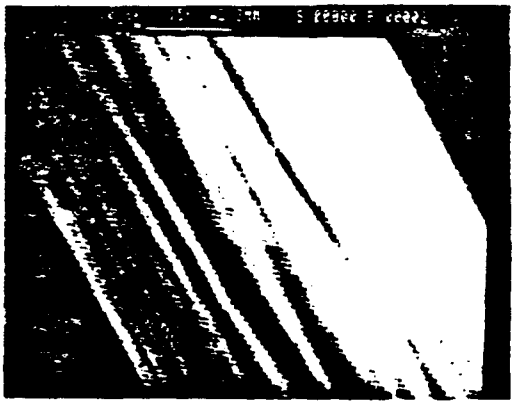

Fig. 11. SEM photograph showing the fibrillar structure in PAN-based carbon fibers (1000°C).

(a)

(b)

Fig. 12. The ribbon-like morphology composed of fibrillar structure in PBZT-based carbon fibers processed at (A) 850°C and (B) 1600°C.

Scanning electron microscopy observations reveal some of the features of the PBZT-based carbon fibers (Fig. 10). The morphology is distinctly fibrillar, but the fibrils are a little finer than those in the PAN-based carbon fibers (Figs. 10 and 11). The origin of these fibrils is clearly in the morphology of precursors (Fig. 2). There is a well defined sheath-core structure that is often observed and also a skin on the sheath with a ribbon-like morphology (Figs. 12 and 13). It is not clear yet whether these arise from diffusion-dominated aspects of coagulation in precursor fiber formation or reactions at the carbonization stage. It should be noted that the size of the precursor fiber (about 20 μm dia.) is much larger than that of typical high-performance carbon fiber precursors (about 7 μm dia.), thus making it highly susceptible to the formation of a sheath-core structure. The surface of PBZT-based carbon fibers contains gross defects, such as the longitudinal striations and microvoids shown in Fig. 14, which are also seen in precursors (Fig. 2). The microvoids between the fibrils (Fig. 14B) could have resulted from separation of the fibrils caused by the simultaneous loss of mass and densification that occur during carbonization. If such defects and the high concentration of microvoids that are created during carbonization/consolidation can be reduced significantly, these new fibers can be used to expand the experimental domain for studies of morphology-property relations in carbon fibers. For example, the distinctly finer scale of fibril formation in the PBZT-based fibers would allow examination of one of the mechanisms that has been proposed for failure in axial compression, namely, microfibrillar buckling[9]. It is necessary, however, that the gross defects predominant in the current fibers be eliminated before a valid study of such aspects can be conducted. It should also be noted here that consolidation defects could have been generated in processing due to the large diameter of the PBZT precursor fibers (Tables 1 and 3).

This preliminary investigation has shown clearly that oriented fibers of rod-like poly(*p*-phenylene

(a)

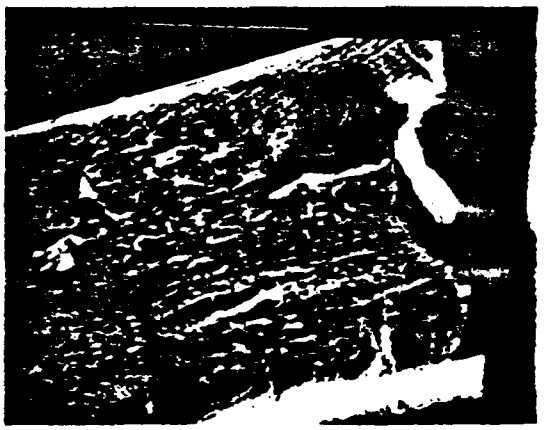

(b)

Fig. 13. The sheath-core structure of the PBZT-based carbon fibers: (A) cross-section (fiber treated at 1600°C); (B) logitudinal profile (fiber treated at 1200°C).

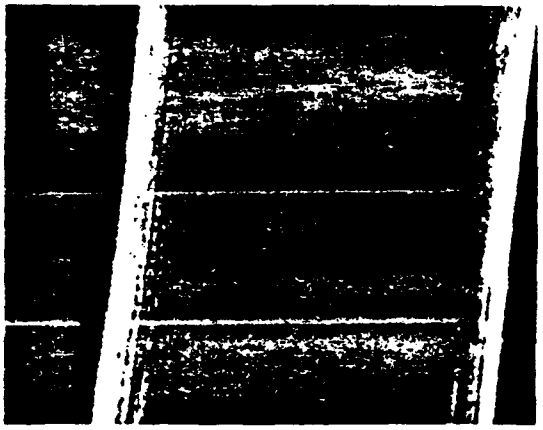

(a)

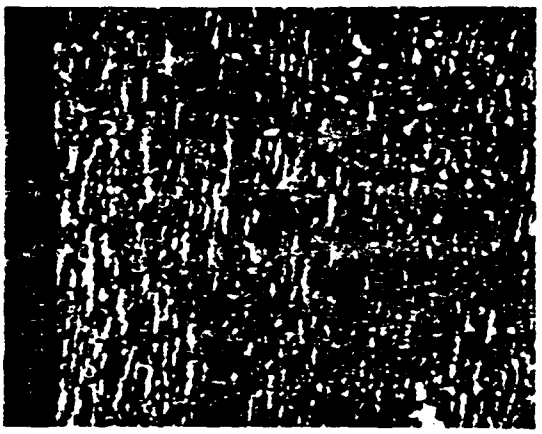

(b)

Fig. 14. SEM photographs, showing defects on the surface of PBZT-based carbon fibers: (A) longitudinal striations; (B) a large amount of microvoids formed between fibrils. (Photographs obtained by Gary Price, University of Dayton Research Institute.)

benzobisthiazole) can be converted cohesively to carbon fibers. It offers a mechanism by which carbon fibers with different morphological parameters, especially in the scale of evolution of morphological units, can be obtained. It is necessary, however, to eliminate the defects in the precursor fibers that are currently available before these can be used in studies of morphology-property relations in carbon fibers.

Acknowledgements—The work reported here was supported by a grant from the U.S. Air Force Office of Scientific Research (AFOSR-89-0193). The authors thank Mr. Gary Price of UDRI for SEM and SAXS photographs, and are also indebted to Mr. Sundar Damodaran for his assistance in some experiments.

REFERENCES

1. R. Bacon. In *Chemistry and Physics of Carbon*, Vol. 9 (Edited by P. L. Walker, Jr. and P. A. Thrower) pp. 1–102. Marcel Dekker, New York (1973).
2. *Graphite Fibers and Filaments*, (Edited by M. S. Dresselhaus, G. Dresselhaus, K. Sugihara, I. L. Spain, and H. A. Goldberg) pp. 4–9; pp. 14–16; pp. 35–79. Springer-Verlag, Berlin (1988).
3. *Carbon Fibers* (Edited by Jean-Baptiste Donnet, and R. C. Bansal), pp. 12–26; pp. 37–42; pp. 163–199. Marcel Dekker, Inc., New York (1981).
4. *Strong Fibers* (Edited by W. Watt and B. V. Perov), pp. 389–471; pp. 495–538. Elsev. r Sci. Publish Co. Inc., Amsterdam (1985).
5. H. M. Ezekiel, *Applied Polymer Symposium* **9**, 315 (1969).
6. U. S. Patent 3,528,774 (1970).
7. I. Tomizuka, Y. Isoda, and Y. Amamiya. *Tanso* **106**, 93 (1981).
8. I. Tomizuka, K. Ogawa, and Y. Tanaka. *Tanso* **115**, 155 (1983).
9. S. Kumar and T. E. Helminiak, *MRS Symposium* **134**, 363 (1989).
10. M. K. Jain and A. S. Abhiraman, *J. Mater. Sci.* **22**, 278 (1987).
11. M. K. Jain, M. Balasubramanian, P. Desai, and A. S. Abhiraman, *J. Mater. Sci.* **22**, 301 (1987).
12. M. Balasubramanian, M. K. Jain, S. K. Bhattacharya, and A. S. Abhiraman, *J. Mater. Sci.* **22**, 3864 (1987).
13. W. W. Adams and R. K. Eby, *MRS Bulletin* **XII**, 22 Nov./Dec. (1987).
14. S. R. Allen, *J. Mater. Sci.* **22**, 853 (1987).
15. S. R. Allen, Ph.D. Dissertation, U. Mass., Amherst, MA (1983).
16. H. Jiang, Ph.D. Dissertation, The Johns Hopkins Univ., Baltimore, MD (1989).
17. C. S. Wang, S. J. Bai, and B. P. Rice, *ACS PMSE Proceedings, Washington, DC* **60**, 767 (1989).

ANALYSIS OF TENSILE RECOIL METHOD FOR THE COMPRESSIVE STRENGTH MEASUREMENT OF PAN-BASED CARBON FIBERS

Hao Jiang, S. Damodaran, P. Desai, S. Kumar, A. S. Abhiraman,
Polymer Education and Research Center,
and K. Tsui, School of Industrial & Systems Engineering,
Georgia Institute of Technology, Atlanta, GA 30332

Introduction

Carbon fibers occupy a premier position among high performance fibers for composites. Its properties in compression, although superior to most of other fibers, is still relative poor in comparison to tension. A considerable effort is currently being made to understand the morphological features which govern the compressive behavior of these fibers. A problem in such efforts arises from the absence of a satisfactory method for the single fiber compressive strength. Since the fiber diameter is so small (5-10 μm) it is very difficult to apply a true axial compressive stress to a single fiber without buckling. Some indirect measurements, such as bending beam and elastica loop tests, estimate compressive strength values much higher (about 2-3 times) than those determined in composites [1-3]. The test of embedding fibers (or single fiber) in the matrix in some cases appears to provide a better agreement but is affected by the residual stress on the tested fibers caused by the matrix shrinkage, the alignment of the fibers during the test and the tedious procedures [4,5].

It has been reported that the compressive strength measured by the tensile recoil method for high-performance polymer fibers gave an excellent agreement with values obtained from composite tests [6]. The objective of this work is to use the recoil method to measure the compressive strength of PAN-based carbon fibers, to find its suitability, limitations and failure mechanism. Different statistical models, such as Weibull and logistic, were used to analyze the censored recoil-test data in order to obtain the true distribution of the cumulative compressive failure and to determine the compressive strength. The recoil method is also used to examine the evolution of compressive strength during carbon fiber formation.

Tensile Recoil Method

The specimen used was a PAN-based carbon fiber treated at 1000°C with a diameter of 7.3 μm. A modified single filament recoil method was adopted for compressive strength test [7]. Three different fiber gauge lengths, 0.5", 1" and 3", were used. The fibers were stretched in the Instron (Model 1125) using a 500g load cell to a desired tensile stress level, and then cut by an electric spark at the center of the gauge length. Both halves of the tabs with remaining fibers were carefully collected from the clamps for examination to ascertain whether or not fracture occurred due to the recoil stress and the event at each tab was recorded accordingly. The testing equipment and procedure are detailed in ref. [8]. For each stress level, 20 to 40 filaments were tested. The tension was increased in steps of 0.5 g force for 1" and 3" gauge length samples and 1 g force for 0.5" GL sample (1 g force corresponded to 0.23 GPa stress).

Fig. 1 shows the results of the recoil measurements for the PAN-based carbon fibers. With increasing applied tension, more specimens were broken at the end-tabs during the tests. The results of the recoil tests for PAN-based carbon fibers are seriously influenced by the variation of gauge length, especially at gauge lengths longer than 1.0".

Major assumptions in the theoretical foundation of the recoil method are (1) the test sample is a homogeneous, linearly elastic material; (2) the sample is clamped rigidly at each end of the gauge length; (3) the sample has an initial uniform tensile stress along its length except at the free ends created by cutting; (4) the energy dissipation during the recoil is so small as to be neglected. However, in practice, the specimen could be nonuniform both in longitudinal and lateral directions with flaws and defects. The glue for fixing fiber at the end-tabs and the electric spark for cutting the fiber could both give rise to an unbalanced movement of the specimen. All these factors could cause fiber bending during the test. Fig. 2 is a SEM photograph of the fiber cross-section after recoil failure. It is similar to the morphology produced by bending failure. The morphology appears to be divided into two different types, apparently corresponding to failure in compression and in tension [9,10]. Most of the recoil-damaged fibers exhibit this kind of phenomenon. For reasons which are not yet fully understood, the "recoil" strength distribution obtained with 1" and 0.5" gauge lengths were closer to each other than the distribution obtained with a 3" GL.

The recoil test does not provide a direct measure of the compressive strength. Instead, it provides the fraction of specimens that fail under a given recoil stress, i.e., the fraction of specimens that possess a "recoil" strength less than the applied stress. These measurements can be considered as censored data of the compressive strength. The goal is to characterize the statistical distribution of the compressive strength based on the censored data. Two frequently used statistical models, logistic and Weibull, were chosen. For the logistic model,

$$F(x_i) = \frac{exp(\beta_0 + \beta_1 x_i)}{1 + exp(\beta_0 + \beta_1 x_i)}$$

where x_i is the recoil stress put on the fiber for the ith experiment. $F_i(x)$ is the model estimation of the failure ratio under a stress x_i. β_0 and β_1 are model parameters. For Weibull model,

$$F(x_i) = 1 - exp\left\{-\frac{(x_i - \alpha_0)^{\alpha_2}}{\alpha_1}\right\}$$

where α_0, α_1 and α_2 are model parameters.

In order to estimate the unknown parameters, two methods were used to fit the experimental data with the above models, the least squares and the maximum likelihood. The object functions for the two are

$$S_{lsq} = \sum_i^m \left(F(x_i) - B_i\right)^2 \rightarrow \text{minimized}$$

$$S_{lklh} = \prod_i^m F(x_i)^{y_i} \left(1 - F(x_i)\right)^{(n_i - y_i)} \rightarrow \text{maximized}$$

where m is the total test points for a certain gauge length, B_i is the experimental fiber broken ratio under the stress x_i, y_i is the number of broken fibers under stress x_i and n_i is the total number of tested fibers under stress x_i. So, $B_i = y_i / n_i$. Because of the very large values of S_{lklh}, the object function was transformed to $\log(S_{lklh})$ for the calculation.

For both models, the parameters calculated by the least square and by the max. likelihood are similar to each other verifying the selection of the parameters (Table I). Fig. 3 shows the fitting results. The fitted curves are very close to each other, perhaps suggesting that the cumulative failure ratio tested with the recoil method could be described by either the logistic or the Weibull model. On the other hand, it is possible that the total number of specimens is not large enough to distinguish the difference between the two models.

Additional details of the recoil method pertaining to the following will be presented at the conference.

(1) a universal model including the gauge length dependence;
(2) regression of compressive strength;
(3) design of the experiment;
(4) failure modes.

Evolution of Structure & Properties in Carbonization

Although the recoil test is subject to multiple modes of failure and yields censored data, it is still a valuable technique for comparison at short gauge length. It is being employed to study the evolution of compressive properties during formation of carbon fibers from PAN-based precursors.

Carbon fiber manufacture from polyacrylonitrile consists of low temperature stabilization followed by carbonization at temperatures which are typically above 1500°C. Significant evolution of properties (tensile, compressive, electrical and thermal) occur during this operation. Therefore, another focus of this study has been on the evolution of mechanical properties during carbonization in order to obtain an optimum combination of tensile and compressive properties.

Experiments have been performed using 'on-line' samples from a 1600°C carbonization operation, where the fiber was quickly withdrawn from the entrance side of the furnace after being cut at the exit point of the furnace. Fig. 4 shows the results of tensile and compressive strength measurements of fiber samples which had experienced varying extent of carbonization. The development of compressive strength appears to occur within the same time-temperature range as in the case of tensile strength. Typically a maximum value for tensile strength is observed around 1700°C and indicates a

transition from morphology-controlled behavior to impurity-generated flaw-controlled behavior of tensile strength. Similar studies on fibers carbonized at different carbonization temperatures will be presented. The development of compressive and tensile strengths will be correlated to the concomitant morphological and chemical changes in the fiber.

Acknowledgments:

The authors acknowledge gratefully the contributions from Ms. Elaina McKoy who made some of the recoil strength measurements. The work reported here has been supported by the U.S. Air Force Office of Scientific Research and the Georgia Tech Polymer Program Associates.

Bibliography

1. D. Sinclair, *J. Appl. Phys.*, **21**, 380 (1950).
2. S. DeTeresa, *J. Mater. Sci.*, **19**, 57 (1984).
3. S. Kumar and T.E. Helminiak, *Mat. Res. Soc. Symp. Proc.*, **134**, 363 (1989).
4. H.M. Hawthorne and E. Teghtsoonian, *J. Mater. Sci.*, **10**, 41 (1975).
5. L. Drzal, AFWAL-TR-86-4003 (1986).
6. S.R. Allen, *J. Mater. Sci.*, **22**, 853 (1987).
7. C.S. Wang, S.J. Bai and B.P. Rice, *Proc. ACS Div. Polym. Mat. Sci. Eng.*, **61**, 550 (1989).
8. S. Damodaran, et al., to be published.
9. M.G. Dobb, D.J. Johnson and C.R. Park, *J. Mater. Sci.*, **25**, 829 (1990).
10. A.S. Crasto and S. Kumar, *Intl. SAMPE Proc.*, **35**, 318 (1990).

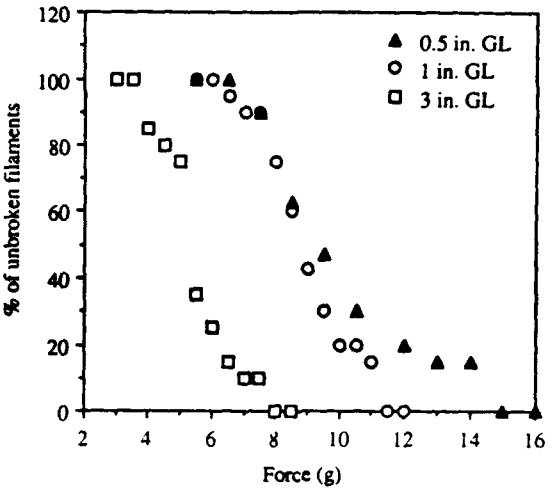

Fig. 1. Effect of gauge length on recoil compressive failure.

Table I. Comparison of Model Parameters with Different Fitting Methods.

	Logistic		Weibull		
Fitting Method	β_0	β_1	α_0	α_1	α_2
Least Square	-9.4	4.6	1.2	0.85	2.6
Maximum Likelihood	-10.0	4.9	1.2	0.87	2.5

Fig. 2. Typical cross section of carbon fibers after recoil fracture.

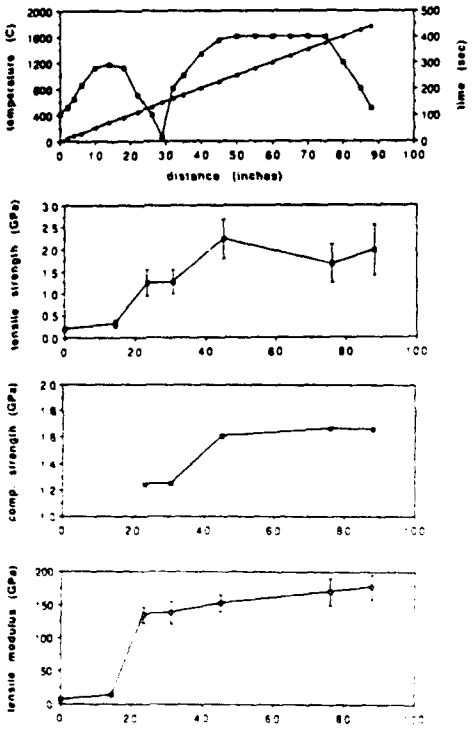

Fig. 4. Evolution of mechanical properties during carbonization of a PAN-based precursor at 1600°C.

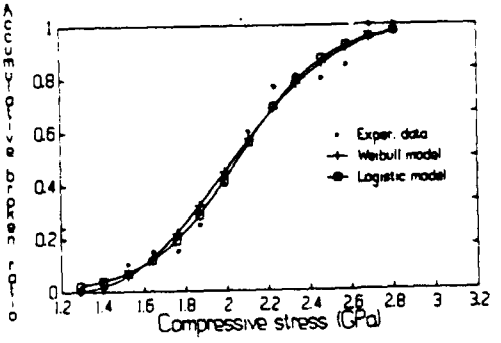

Fig. 3. Comparison of Logistic and Weibull distributions using maximum likelyhood method for parameter estimation. Fiber gauge length = 1.0 in.

PMSE POLYMERIC MATERIALS SCIENCE AND ENGINEERING

VOLUME 64

SPRING MEETING 1991
ATLANTA, GEORGIA

PROCEEDINGS OF THE AMERICAN CHEMICAL SOCIETY
DIVISION OF POLYMERIC MATERIALS: SCIENCE AND ENGINEERING

Analysis of Failure in 'Recoil From Tension' of PAN-based Carbon Fibers

Hao Jiang[1], A. S. Abhiraman [1], and K. Tsui[2]

Polymer Education and Research Center

GEORGIA INSTITUTE OF TECHNOLOGY

Atlanta, GA 30332

[1]School of Chemical Engineering

[2]School of Industrial and Systems Engineering

Abstract

Results from a study of the "recoil from tension" method for estimating the compressive strength of the polyacrylonitrile (PAN)-based carbon fibers are reported here. Analysis of the effect of different gauge lengths on the recoil strength distribution and the fracture morphological features of cross-sections of the tested filaments imply that both axial recoil and bending influence the recoil failure of PAN-based carbon fibers.

The experimental recoil strength distributions have been compared to logistic and weibull models. A universal logistic model that incorporates a dependence on gauge length has been found to provide a good fit to the distributions obtained at different gauge lengths. This analytical expression can be used to obtain a physically meaningful extrapolated average "zero gauge length" recoil strength which might be appropriate for estimating the true axial compressive strength of fibers.

1. Introduction

Carbon fibers occupy a premier position among high performance fibers for composites. Their properties in compression, although superior to most of the other fibers, are still relatively poor in comparison to tension. A considerable effort is currently being made to understand the morphological features which govern the compressive behavior of these fibers. A problem in such an effort arises from the absence of a satisfactory technique for measurement of the single fiber compressive strength. Since the fiber diameter is small (5-10 μm), it is very difficult to apply a true axial compressive stress to a single fiber without causing buckling[1-3]. Some indirect measurements, such as bending beam and elastica loop tests, estimate compressive strength values much higher (about 2-3 times) than those determined in composites[4-6]. Tests with embedded fibers (or single fiber) in the matrix appear to provide a better agreement in some cases, but are affected by the residual stress on the tested fibers caused by the matrix shrinkage, the alignment of the fibers during the test and the tedious procedures[7-11].

The compressive stress developed during retractive deformation of a fiber initially subjected to a tensile stress was described by Allen[12]. In the absence of viscous damping, the compressive stress developed at the fixed end is assumed equal in magnitude to the initially imposed tensile stress. The pretensioning is facilitated in actual testing by stretching the fiber and cutting it in the middle, thereby allowing both segments to undergo the recoil process. The strength of high performance fibers measured by this "recoil from tension" (RFT) method has been reported to agree well with the compressive strengths obtained from composite tests[1,2,6,12,13]. Extensive recent investigations in our laboratories[14-16] with PAN-based carbon fibers obtained by carbonization over a broad range of temperature (800° - 2800°C) also reveal an excellent correlation between the average recoil strengths and the axial compressive

strengths measured in uniaxially oriented composites.

The main objective of the work reported here is to explore the morphological and statistical features of failure of PAN-based carbon fibers in RFT test. A physically meaningful statistical model that can provide a link to the performance of these fibers in axial compression of composites is sought.

2. Experimental

2.1 Materials

The materials used in the study are PAN-based carbon fibers, produced by carbonization at 1000°C. These fibers were chosen from a range of carbon fibers[16] for conducting a thorough analysis of the RFT method because their axial compressive strengths are representative of the upper end of performance in carbon fibers. Some properties of these fibers are given in Table 1.

2.2 Single Fiber Tensile Tests

The carbon fiber specimens were mounted on thin cardboard tabs at a gauge length (GL) of 1" by using a quick-gel glue. The samples were extended to failure on an Instron (Model 1125)tensile tester at a rate of 0.05 in/min (5 %/min), using a 500g load-cell to measure the forces. At least 10 filaments were chosen randomly for testing from each sample fiber bundle. The crosssections of the samples were assumed to be perfectly circular in the calculation of applied stresses.

2.3 Single Fiber "Recoil From Tension" (RFT) Tests

A modified single filament RFT method was adopted for the measurements[13]. The sample-making technique is the same as that used in tensile measurements. The fibers were tested at three different gauge lengths, 0.5" (1.27 cm), 1" (2.54 cm) and 3" (7.62 cm). The fiber samples were extended to a desired tensile stress level and then cut rapidly by the application of an electric spark at the center of the gauge

length. Each tab with its remaining fiber segment was then carefully collected from the clamps for examination to ascertain whether or not fracture had occured during recoil and the event at each tab was recorded accordingly. Details of the test scheme are shown in Fig. 1[15,16]. 20 to 40 filaments were tested at each applied stress level. The tension was increased in steps of 0.5 g force for 1" and 3" gauge length samples and 1 g force for 0.5" gauge length sample (1 g force corresponded to ~0.23 GPa stress). It should be noted that nearly all recoil failures occured in the region close to the tab-ends.

A difficulty with performing the RFT test arises from premature tensile failure, i.e., failure prior to reaching the desired tensile stress level. The recoil process following such a tensile failure leads almost invariably to additional failure. The range of stress corresponding to tensile failures extends well below the upper extremum in recoil strength distribution (Fig. 2). Since most tensile failures are initiated at near surface flaws in carbon fibers, the propagation of fracture will result in asymmetric release of stress and thus to a complex stress distribution during recoil. The fact that recoil subsequent to premature tensile failure almost *always* leads to additional failure is a clear indicator of its lack of correspondence to the controlled RFT test. These data were, therefore, not included in the RFT strength distribution data.

2.4 Scanning Electron Microscopy (SEM)

The specimens were sputter-coated with a thin layer of Au-Pd alloy and observed in a Cambridge Stereoscan 90 SEM operating at 15 kV.

3. Results and Discussion

Fig. 3 shows results of the RFT measurements obtained at different gauge lengths. In obtaining the strength distributions shown here, each of the two recoiling segments that resulted from cutting the filament was regarded as a separate sample. The fail-

ures recorded at only one or both jaws in these tests were also recorded appropriately.

3.1 Recoil Fracture Morphologies and Mechanisms

The recoil fracture surfaces and the longitudinal surfaces near the fractured cross-sections of the carbon fibers after RFT were observed carefully by SEM. Extensive observations were made with the fractures obtained at 0.5" gauge length samples. The 0.5" GL samples were chosen because they cover the widest applied tensile stress region (from 1.29 to 3.79 GPa; Fig. 3) and are thus likely to provide maximum information regarding variations in fracture morphology.

As many as seven different fracture morphologies could be observed with the SEM.

TypeI: Consists of striations radiating from the failure point, similar to the typical features of brittle failure of PAN-based carbon fibers in tension[17,18]. The clear location of the failure point at the edge of the fracture surface (Fig. 4) shows that failure had initiated in this case at a surface flaw on the fiber.

TypeII. There are clearly two separate parts, a rough striated one which is similiar to type I and occupies most of the area, and a narrow relatively smooth one (Fig. 5).

TypeIII. The rough area and the smooth area are nearly equal. In addition, it also exhibits a rather deeply corrugated zone between the two areas (Fig. 6).

TypeIV. The morphology looks similar to Type II or Type III, but there is a flaw at the surface edge of the smooth area near the filament surface (Fig. 7).

TypeV. There are two rough striated zones on two opposite sides of the fracture cross-section (Fig. 8). The center part, either concave or convex, splits off in the fiber axis direction.

TypeVI. Two smooth and slightly ridged zones which are similar to the smooth area in Type II and III morphologies are seen in different directions (Fig. 9).

TypeVII. Exhibits clear evidence of internal flaws on the fracture surface (Fig.

10).

The relative occurences of the above-mentioned recoil fracture surfaces can be seen in the data given in Table 2. Type II and III are the two most dominant morphologies created by failure in the RFT test.

The theoretical basis[12] for equating the recoil strength to the fiber axial compressive strength is based on the following assumptions: (1) The test sample is a homogeneneous, linearly elastic material. (2) The sample is clamped rigidly at each end. (3) At the instant the sample is cut, it has a uniform tensile stress along its length except at the free ends created by cutting. (4) The energy dissipation prior to failure in recoil is negligible. In practice, however, the specimens could be nonuniform both in longitudinal and lateral directions, and also have variations in diameter and shape. Improper fixing of the fiber at the tabs, any misalignment of the specimen, or asymmetry in cutting by the electric spark could give rise to an unbalanced moment and cause fiber bending during recoil. If bending occurs, both the fiber length and the applied stress would influence failure. It is apparent that except Type I, all the other recoil fracture surfaces (which constitute about 90%) have the topography with some morphological features associated with a contribution to failure from bending[17-26]. The fracture surface contains a rough portion characteristic of failure in tension and a region that reveals compressive failure with its smooth morphology. Any bending during recoil is likely to make the region near the clamp most susceptible to failure. However, the complexity of the internal and external factors governing the bending during recoil makes it difficult to control, or even account for, the stress distributions and any resulting failures accurately. The myriad of fracture surfaces resulting from this test (Figs. 4 - 10) exemplifies this aspect. The following should be regarded, therefore, as only a simplified qualitative rationalization of the effects of the applied tension, bending and recoil compression on the mechanisms of fiber failure in the

RFT tests.

The recoil process can be considered to consist of three stages. In the first stage, immidiately after the fiber is cut, both segments begin to recoil. If there is a significant bending at this stage, the whole fiber cross-section would be still under tension, albeit non-uniform. If the fiber should break at this stage its fracture surface would reveal only a tension mode failure morphology, just as in type I (Fig. 4). Type I morphology is rarely found at longer gauge lengths, e. g., at 3 inch. Also when compared to the whole stress range of recoil failure at 0.5 inch gauge length, the stress level for type I failure is still low (Table 2). The high fraction of premature tensile failure, i.e., during the pretensioning phase of the test, at the higher stress levels (Fig. 2) appears to be responsible for this aspect in the distribution of recoil failure morphologies.

The recoil failure morphologies I, II, III, V and VI displayed in Figs. 4, 5, 6, 8 and 9 indicate, respectively, failures at possibly successive stages of the recoil process. Type II is characteristic of failure with a contribution of bending and tension producing a small zone of compression in the cross-section, while type III shows failure at a relatively higher level of recoil stress and bending. Morphologies V and VI show clearly features that point to a smooth or random lateral oscillation of the fiber having occured prior to complete failure.

Some of the fibers exhibit kink bands on the fiber surface near the tab ends, close to the fracture surface (Figs. 6 and 11). It is not clear whether a kink band formed on the compressive side during initial bending and/or recoil might have served as a site for initiation of tensile failure during subsequent oscillation. Some of the kink bands have propagated all the way around the fiber circumference, indicating at least some oscillation prior to complete failure.

The guage length effect on recoil strength (Fig. 3) is also a strong evidence of fiber bending during the RFT test. As described above, the most severe recoil damage

always occurs in the region close to the tab ends because of bending. With increasing gauge length, the bending stress produced in the region near the tab would increase too, thus contributing to a decrease in the observed recoil strength. The mechanism of decrease in recoil strength with increase in gauge length is clearly different from the mechanism operational in tensile testing. Increasing gauge length produces a higher stress in the same region (near the tab) in recoil with bending, contributing to an apparently lower recoil strength, whereas the decrease in tensile strength at longer gauge lengths is well known to be due to a higher probability of finding failure-causing flaws within the test volume. The statistical analysis given in the following provides a possible mechanism for estimating a "bending-less" recoil strength from RFT test data obtained at different gauge lengths.

3.2 Statistical Models

Two simple methods are widely used in routine work to obtain the recoil strength from the RFT test. One is to find the recoil failure range and then choose the average value of its superior limit (the lowest stress level at which fibers always suffer recoil failure) and inferior limit (the highest stress level at which the fiber can always sustain recoil without failure) as the recoil strength. The other is to find a stress around which ~50% fibers suffer recoil failure. The following analysis, while being more vigorous, requires more extensive experimentation than the above-mentioned simple methods.

Repeated recoil test provides the fraction of specimens that fail under a given recoil stress, i.e., this fraction of specimens possesses a recoil strength *less than* the applied stress. During the recoil test, after the fiber is cut at the center of the gauge length, there exist two separate recoil processes in the upper and lower fiber segments. If it is assumed that the recoil failure at each tab-end is an independent event and governed by the same probability distribution, $F\{\sigma\}$ = Probability{Recoil strength$\leq \sigma$}, where σ is the recoil stress,

the Probability{Failure at only one tab-end}, $g_1\{\sigma\}$, should be given by

$$g_1\{\sigma\} = 2F\{\sigma\}[1 - F\{\sigma\}],$$

the Probablity{ Failure at both ends}, $g_2\{\sigma\}$, should be

$$g_2\{\sigma\} = F\{\sigma\}F\{\sigma\}, \text{ and}$$

the Probability{ No failure }, $g_o\{\sigma\}$, should be

$$g_o\{\sigma\} = [1 - F\{\sigma\}]^2.$$

The assumption of independent failure processes at the two tabs seems reasonably justified by the experimental results (Fig. 12). With increase of the applied stress, the probability of fiber recoil failure at only one tab-end, $g_1\{\sigma\}$, increases at the beginning and, after reaching its maximum, it gradually decreases to zero. The distribution of fiber recoil failure at both tab-ends, $g_2\{\sigma\}$, increases monotonically from 0 to 1 with the applied stress. It should be noted, however, that a small but systematic difference can be observed when the distributions of breaks at the upper and lower jaws are considered separately (Fig. 13). The fiber segments appear to be slightly more prone to failure at the upper jaw in the shorter GL (0.5 inch) samples and at the lower jaw in the longer GL (3 inch) samples. Visual observations during these tests suggest the probable reasons for these differences to be the greater influence from the propagation towards the upper jaw of the flame that arises from cutting the fiber with the electric spark in the case of the shorter GL samples and the role of gravity in causing bending of the lower recoiling segment in the case of the longer GL. The observed differences are, however, not large enough to be of practical significance. The data from both tab ends were, therefore, pooled into a single population in the statistical analysis to identify an appropriate probablity distribution for recoil failure.

The weibull model which is based on the "weakest link theory" has been widely used for characterizing the tensile strength distribution of PAN-based carbon fibers[27-32]. The recoil test has, however, a different foundation from the tensile test. Failure

in the RFT test occurs almost exclusively at the part close to the tab-ends, i.e., the breakage is not necessarily at the weakest link point along the recoiling fiber segment. Therfore, in exploring the recoil strength distribution, the logistic distribution is compared with the weibull distribution to fit the experimental data[30,33].

For the logistic model,

$$F(\sigma) = \frac{e^{\beta_o+\beta_1\sigma}}{1+e^{\beta_0+\beta_1\sigma}}$$

where σ is the recoil stress applied to the fiber. $F(\sigma)$ is the model estimation of the failure ratio under a stress σ. β_0 and β_1 are model parameters. For the weibull model,

$$F(\sigma) = 1 - exp\{-\frac{(\sigma-\alpha_0)^{\alpha_2}}{\alpha_1}\}$$

where α_0, α_1, and α_2 are all model parameters.

In order to estimate the unkown parameters, two methods, the Least Square and the Maximum Likelihood[33,34], were used to fit the experimental data with the above models. The objective functions for the two methods are

$$S_{ls} = \sum_i^m (F(\sigma_i) - B_i)^2 \longrightarrow Minimized$$

where m is the total test points for a certain gauge length, B_i is the experimental fiber broken ratio under the stress σ_i,

$$S_{ml} = \prod_i^m F(\sigma_i)^{y_i}(1 - F(\sigma_i))^{(n_i-y_i)} \longrightarrow Maximized$$

where n_i is the total number of recoil tests conducted under stress σ_i and y_i is the number of fibers broken in recoil under stress σ_i. Therefore, $B_i = \frac{y_i}{n_i}$. Because of very large values of S_{ml}, the object function was transformed to $\log(S_{ml})$. The Simplex optimization computer software package[35] was used in the regression calculations.

For both models, the parameters calculated by the least square and the maximum likelihood methods were in extremely close agreement. Fig. 14 shows that the fitted curves are close to each other for both models, perhaps suggesting that the experimentally observed failure in the recoil method can be fitted well by either the logistic or the weibull model.

There are several reasons for selecting the logistic instead of the weibull model to establish a universal model that includes the gauge length dependence of failure. The logistic model is one of the most widely used models for describing the relationship between a dichotomous outcome variable and a set of covariates. As described above, the weakest link theory which constitutes the theoretical foundation for using the weibull distribution in describing the strength of materials is not applicable to the recoil test. Also, the following regression analysis with a gauge length-dependent universal logistic model shows that this model can indeed display a clear physical significance in fitting the RFT data.

The universal logistic model with gauge length dependence that has been explored in the context of recoil failures is given by

$$F(\sigma) = \frac{e^{\beta_0+\beta_1\sigma+\beta_2\sigma g_l+\beta_3 g_l}}{1+e^{\beta_0+\beta_1\sigma+\beta_2\sigma g_l+\beta_3 g_l}}$$

where g_l is the length of each segment in the RFT test, i.e., half of the gauge length (cm); β_0 is a shape parameter or the so-called scale parameter; β_1 is a stress parameter (GPa^{-1}), the term $\beta_1\sigma$ expresses the effect of stress; β_2 is a stress-gauge length parameter $(GPa - cm)^{-1}$, the term $\beta_2\sigma g_l$ expresses the interactive effect of gauge length and applied stress; β_3 is a gauge length parameter (cm^{-1}), the term $\beta_3 g_l$ represents the pure gauge length effect. The fitted parameters are given in Table 3. As seen in Fig. 15, the fits obtained at different gauge lengths with a single universal logistic model are as good as those from the individual fittings of the 2 parameter logistic models at each gauge length. In other words, a single universal logistic model that contains gauge length dependence can replace all the separate logistic models at different gauge lengths. It should also be noted that the term $\beta_3 g_l$ is so small that it can be neglected and excellent fits can be obtained with only three parameters (β_0, β_1 and β_2) in the universal logistic model. The fact that gauge length influences recoil strength distribution only interactively with the applied recoil stress is consistent with

the previously inferred role of bending stress near the tab in dictating failure in the RFT test.

The mean recoil strength, $< \sigma >_r$, can be obtained from the distribution, $F(\sigma)$, as

$$< \sigma >_r = \int_0^\infty \sigma f(\sigma) d\sigma = \int_0^\infty [1 - F(\sigma)] d\sigma$$

where $f(\sigma)$ is the probability density function ($f(\sigma) = F'(\sigma)$). If $F(\sigma)$ is the three parameter universal logistic distribution function, we obtain the mean recoil compressive strength as

$$< \sigma >_r = \frac{-\beta_0}{\beta_1 + \beta_2 g_l}$$

An interesting feature in the above equation for mean recoil strength is that it lends itself easily to the estimation of a "zero gauge length" recoil strength. Such an estimate is likely to be representative of a mean axial compressive strength of the fiber because it eliminates the interactive gauge length-recoil stress influence which is believed to represent the uncontrolled bending in the RFT test. An estimate for the zero gauge length axial compressive strength of the fiber, $< \sigma >_c^o$, is thus obtained from the three parameter universal logistic distribution of the recoil strength as

$$< \sigma >_c^o = lim < \sigma >_r = -\beta_0/\beta_1$$

For the fiber analysed here, this average strength is 2.8 GPa. The average zero gauge length tensile strength of this fiber has been estimated to be about 3.9 GPa, i. e., 40% higher than the corresponding estimate in compression from the RFT test. It should also be mentioned here that the more commonly reported way of estimating the "average" recoil strength is by equating it to the mid point between the lowest and the highest recoil stresses at which all the samples fail and all the samples survive, respectively[1,2,6,12-16]. Such an estimate for the fiber studied here is 2.06 GPa at a gauge length of 1", considerably lower than the value of 2.56 GPa that is obtained as the true statistical average of the measured distribution of recoil strengths at this

gauge length. Thus the commonly used method tends to underestimate the average recoil strength.

Concluding Remarks

The "recoil from tension" (RFT) test is being applied increasingly in the evaluation of axial compressive strength of high performance fibers, especially carbon fibers[1,2,6,12-16,25,36]. Extensive work in our laboratories[14-16] and elsewhere[1,2,6, 13,25,36] has shown this method to be valuable in establishing a reliable indicator of changes in axial compressive strength of these fibers. Direct measurement of the latter is considerably more tedious and less reproducible in comparison with the RFT test. The study reported here was carried out to provide an appropriate framework for useful statistical analysis of the RFT test data. The following should be noted in this regard.

(1) The distribution of recoil strengths at a given test gauge length can be fitted well with weibull as well as logistic distributions. However, a universal logistic distribution can provide a physically meaningful framework for quantifying the distribution of recoil strengths as a function of gauge length.

(2) The experimentally observed decrease in recoil strength at longer gauge lengths should not be attributed to any "weak link"-based phenomenon, since failure in recoil occurs almost invariably in the zone close to the tabs to which the fiber is glued. The observed decrease is believed to be the consequence of higher bending stresses at longer gauge lengths. Support for this aspect is seen in regression analysis of RFT test data with a universal logistic distribution that reveals the predominant gauge length dependence to arise only through its interaction with the applied recoil stress.

(3) The universal logistic distribution with interactive gauge length-stress dependence allows a physically meaningful estimation of average recoil strength at zero

gauge length (ZGL). Further research is necessary to determine if such an estimate corresponds to a ZGL estimate of true axial compressive strength.

(4) An overwhelming majority of RFT fracture surfaces of the PAN-based carbon fibers shows clearly a contribution from bending to failure. It is therefore inappropriate to consider the measured average recoil strength to be the axial compressive strength of these fibers at the corresponding gauge length. Nevertheless, the correlations observed experimentally to date[15,16] and the possibility of estimating a ZGL recoil strength that eliminates bending-related terms represent good reasons for continued use and further exploration of this relatively simple method for estimating the potential performance of carbon fibers in axial compression.

Acknowledgements

The authors acknowledge gratefully the numerous insightful discussions with Dr. Prashant Desai of Georgia Tech. They also express their appreciation to Ms. E. McKoy who made some of the recoil measurements and to Dr. Steve Smith (Courtaulds Co., U. K), Dr. Charles Lee and Dr. U. Santosh (U. S. Air Force Office of Scientific Research), and Dr. Satish Kumar and S. Damodaran(Georgia Tech) for useful discussions. The work reported here was supported by the AFOSR and the Georgia Tech Polymer Program Associates.

Figure Captions

Fig. 1: The recoil from tension (RFT) method; (A) the test apparatus; (B) different possibilities after cutting the fibers.

Fig. 2: Fraction of fibers breaking in tension during the recoil test procedure at different stress levels: (gauge lengths: 0.5 inch; 1 inch and 3 inches).

Fig. 3: Effect of gauge length on distribution of recoil failures.

Fig. 4: Typical Type I fracture surface, with striations radiating from a surface flaw as a failure point (shown by an arrow) (the applied recoil stresses: (A) 2.23 GPa and (B) 2.46 GPa).

Fig. 5: Typical Type II fracture surface. The rough area occupies most of the cross-section. A surface flaw at the edge of the tension side is pointed by arrow; (the applied recoil stresses: (A) 2.23 GPa and (B) 2.46 GPa).

Fig. 6: Typical type III fracture surface with rough part and smooth part nearly equal and a deeply corrugated zone in the center; (the applied recoil stresses: (A) 2.81 GPa and (B) 3.28 GPa).

Fig. 7: Typical type IV fracture surface with defect(s) (indicated by an arrow) at the edge of the compression side; (the applied recoil stress: 2.23 GPa).

Fig. 8: Typical type V fracture surface with two rough areas on both sides of the cross-section (pointed out by arrows in (A)) and a splitting zone in the center; (the applied recoil stresses: (A) 2.23 GPa and (B) 2.81 GPa).

Fig. 9: Typical type VI fracture surface with two smooth areas in different directions (pointed by arrows); (the applied recoil stress: 3.28 GPa).

Fig. 10: Typical type VII fracture surface with internal flaw(s) indicated by arrows; (the applied recoil stress: 1.99 GPa).

Fig. 11: Kink bands on the fiber surface (pointed by arrows); (the applied recoil stress: 2.46 GPa).

Fig. 12: Comparsion of experimental and computed distributions (see text for explanations of $F\{\sigma\}$, $g_1\{\sigma\}$ and $g_2\{\sigma\}$). (Gauge length: A- 0.5 inch; B- 1 inch; C- 3 inches). The computed $g_1\{\sigma\}$ and $g_2\{\sigma\}$ are obtained from experimentally obtained $F\{\sigma\}$.

Fig. 13: Comparison of the fractions of recoil breaks at the upper and lower tab-ends. (Gauge length: A- 0.5 inch; B- 1 inch; C- 3 inches).

Fig. 14: Example of fits of obtained with logistic and weibull distributions (experimental data pertain to failure in the upper jaw at 3" gauge length).

Fig. 15: Fits of individual ($F(\sigma) = \frac{e^{\beta_0+\beta_1\sigma}}{1+e^{\beta_0+\beta_1\sigma}}$) and a universal ($F(\sigma) = \frac{e^{\beta_0+\beta_1\sigma+\beta_2\sigma g_l}}{1+e^{\beta_0+\beta_1\sigma+\beta_2\sigma g_l}}$) logistic distributions to recoil failure data. (Gauge length: A- 0.5 inch; B: 1 inch; C- 3 inches). The parameters in the distributions are given in Table 3.

Table 1. Properties of PAN-based Carbon Fibers (Carbonized at 1000°C)

Diameter	7.3 (μm)
Tensile Strength (at 1" gauge length)	2.62 GPa
Tensile Modulus	143 GPa
Torsional Modulus[16]	20 GPa
Elemental Composition (wt%)	Carbon: 90.1 Hydrogen: <0.5 Nitrogen: 9.4

Table 2. The Distribution of RFT Fracture Morphologies

(tested in GL 0.5")

Applied Stress	Morphological Type (number)							Total
(GPa)	I	II	III	IV	V	VI	VII	Number
1.76	2	-	-	-	-	-	-	2
1.99	2	5	-	-	-	2	1	10
2.23	2	5	1	1	1	-	1	11
2.46	1	7	3	-	2	-	-	13
2.81	1	3	4	-	3	-	-	11
3.05	-	2	8	-	-	1	-	11
3.28	-	1	9	-	1	1	1	13
Total	8	23	25	1	7	4	3	71

Table 3. The Parameters of Universal Logistical Models

Statistical Model	Experimental Detail	Model Parameters			
		β_0	β_1 (GPa^{-1})	β_2 (GPacm)$^{-1}$	β_3 (cm^{-1})
Individual Logistic Model	Gauge Length				
	0.5 inch	-7.34	3.24	–	–
	1 inch	-10.02	4.86	–	–
	3 inch	-8.61	6.30	–	–
Universal Logistic Model	Failure Recorded at				
	Upper tab-end	-9.28	3.51	0.594	0.038
	Lower tab-end	-9.62	3.40	0.772	0.000
	Pooled upper & lower tab data	-9.62	3.42	0.690	0.000

References

[1] W. Huh, S. Kumar, T. E. Helminiak and W. W. Adams, *ANTEC '90*, 1245 (1990)

[2] T. A. Doyne, A. N. Palazotto, T. Schuppe, C. Y-C Lee and C. S. Wang, *Proc. ACS, Div. Polym. Mat. Sci. Engr.*, 63, 982 (1990)

[3] M. S. Macturk, R. K. Eby and W. W. Adams, *Polymer*, 32(10), 1782 (1991)

[4] D. Sinclair, *J. Appl. Phys.*, 21, 380 (1950)

[5] S. DeTeresa, *J. Mat. Sci.*, 19, 57 (1984)

[6] S. Kumar and T. E. Helminiak, *Mat. Res. Soc. Symp. Proc.*, 134, 363 (1989)

[7] H. M. Hawthorne and E. Teghtsoonian, *J. Mat. Sci.*, 10, 41 (1975)

[8] L. Drzal, AFWAL-TR-86-4003 (1986)

[9] T. Ohsawa, M. Miwa and M. Kawade, *J. Appl. Polym. Sci.*, 39, 1733 (1990)

[10] M. Miwa, E. Tsushima and J. Takayasu, *Sen'i Gakkaishi*, 47(4), 171(1991)

[11] M. Miwa, E. Tsushima and J. Takayasu, *J. Appl. Polym. Sci.*, 43, 1467(1991)

[12] S. R. Allen, *J. Mat. Sci.*, 22, 853 (1987)

[13] C. S. Wang, S. J. Bai and B. P. Rice, *Proc. ACS, Div. Polym. Mat. Sci. Engr.*, 61, 550 (1989)

[14] G. Bhat, S. Damodaran, P. Desai, L. H. Peebles, Jr. and A. S. Abhiraman, *6th Annual Polym. Proc. Soc. Meeting*, Nice, France, Apr. 17-20 (1990)

[15] Hao Jiang, S. Damodaran, P. Desai, S. Kumar, and A. S. Abhiraman, *Polym. Prep., PMSE*, 64, 383 (1991)

[16] S. Damodaran, *"Evolution of structure and mechanical properties during carbonization of PAN-based precursor fibers* , Ph. D. Thesis, Georgia Tech., Atlanta, GA, Nov. (1991)

[17] J. L. G. Dasilva and D. J. Johnson, *J. Mat. Sci.*, 19, 3201 (1984)

[18] *"Chemistry and Physics of Carbon"*, Ed. P. A. Thrower, Vol. 20, pp. 46, *'Structure Studies of PAN-based Carbon Fibers'*, by D. J. Johnson, Marcel Dekker, Inc., New York (1987)

[19] Eiki Tsushima, *34th International SAMPE Symposium*, pp.2042 (1989)

[20] J. W. Johnson and D. J. Thorne, *Carbon*, 7, 659 (1969)

[21] Charles P. Beetz, Jr., *Fibre Sci. Technol.*, 16, 45 (1982)

[22] G. A. Cooper and R. H. Mayer, *J. Mat. Sci.*, 6, 60 (1971)

[23] D. J. Thorne, V. J. Gough and G. Hipkiss, *Fibre Sci. and Tech.*, 3, 119 (1970)

[24] K. E. Perepelkin, N. V. Klynchnikova and N. A. Kulikova, *Khimicheskie Volokna*, No.2, pp.36 (1989)

[25] M. G. Dobb, D. J. Johnson and C. R. Park, *J. Mat. Sci.*, 25, 829 (1990)

[26] W. R. Jones and J. W. Johnson, *Carbon*, 9, 645 (1971)

[27] L. H. C. Tippett, *Biometrika*, 17, 364 (1925)

[28] J. Tucker, *Proc. Am. Soc. Testing Mat.*, 45, 952 (1945)

[29] R. Moreton, *Fibre Sci. and Tech.*, 1, 273 (1969)

[30] W. Weibull, *J. Appl. Mech.*, 18, 293 (1951)

[31] J. W. Hitchon and D. C. Phillips, *Fibre Sci. and Tech.*, 12, 217 (1979)

[32] K. K. Phani, *Composites Sci. and Tech.*, 30, 59 (1987)

[33] D. A. Raikowsky, *"Handbook of Nonlinear Regression Models"*, pp. 34 and 46, Marcel Dekker Inc., New York (1989)

[34] J. O. Rawlings, *"Applied Regression Analysis: A Research Tool"*, pp. 153, 237, Wadsworth and Brooks/Cool, Pacific Grove, CA (1988)

[35] Hao Jiang, Microcomputers, No.6, p. 58 (1981)

[36] S. Kumar, SAMPE Proceedings, 35, 2224 (1990)

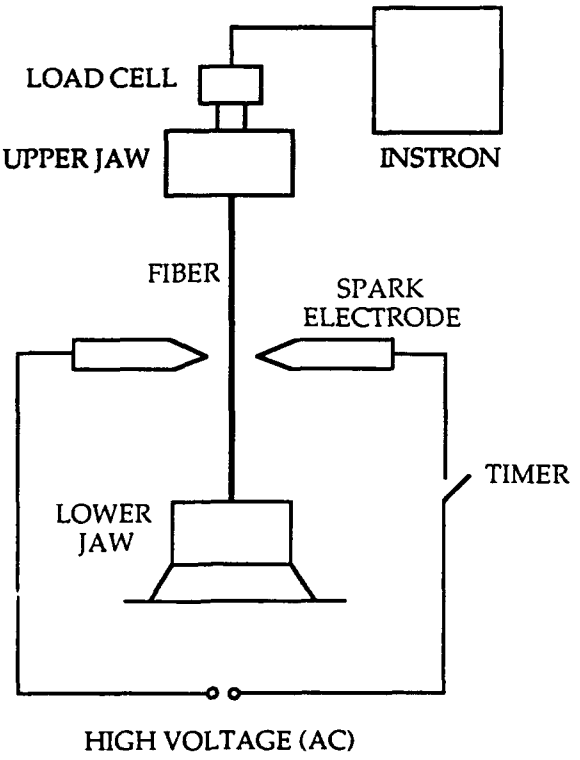
LOAD CELL
UPPER JAW
INSTRON
FIBER
SPARK
ELECTRODE
TIMER
LOWER
JAW
HIGH VOLTAGE (AC)

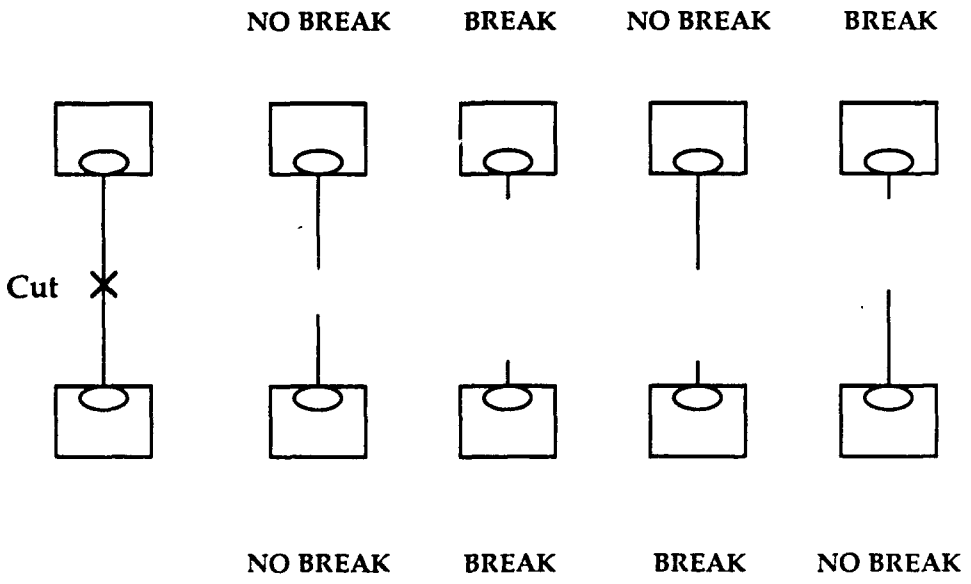
NO BREAK
BREAK
NO BREAK
BREAK
Cut
NO BREAK
BREAK
BREAK
NO BREAK

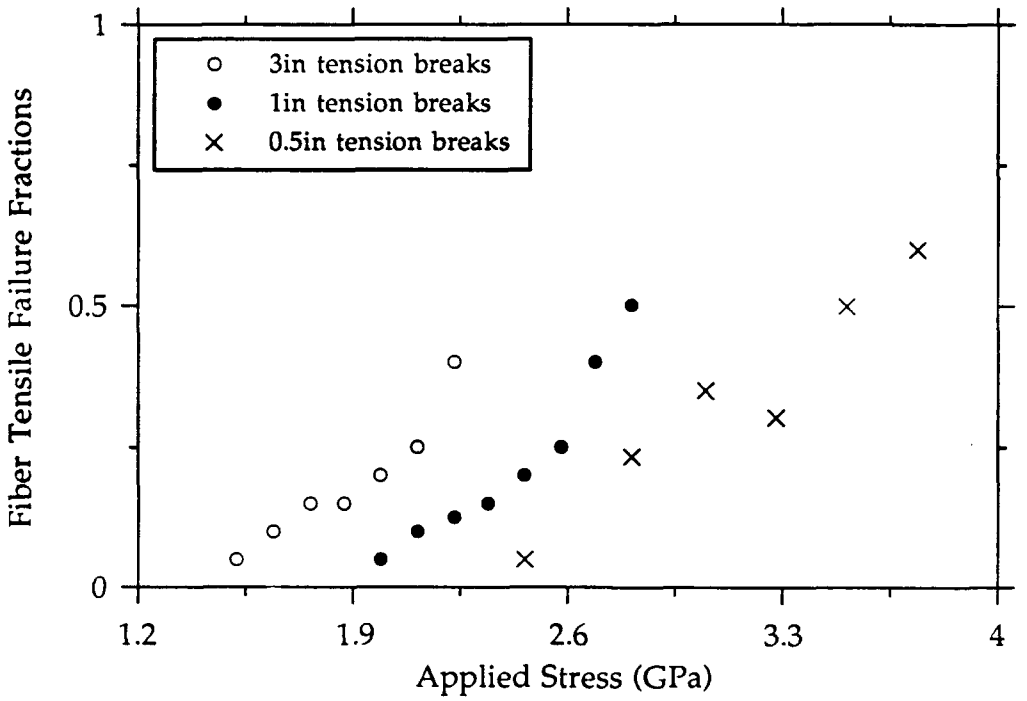
3in tension breaks
1in tension breaks
0.5in tension breaks
Fiber Tensile Failure Fractions
1
0.5
0
1.2
1.9
2.6
3.3
4
Applied Stress (GPa)

Fig. 2

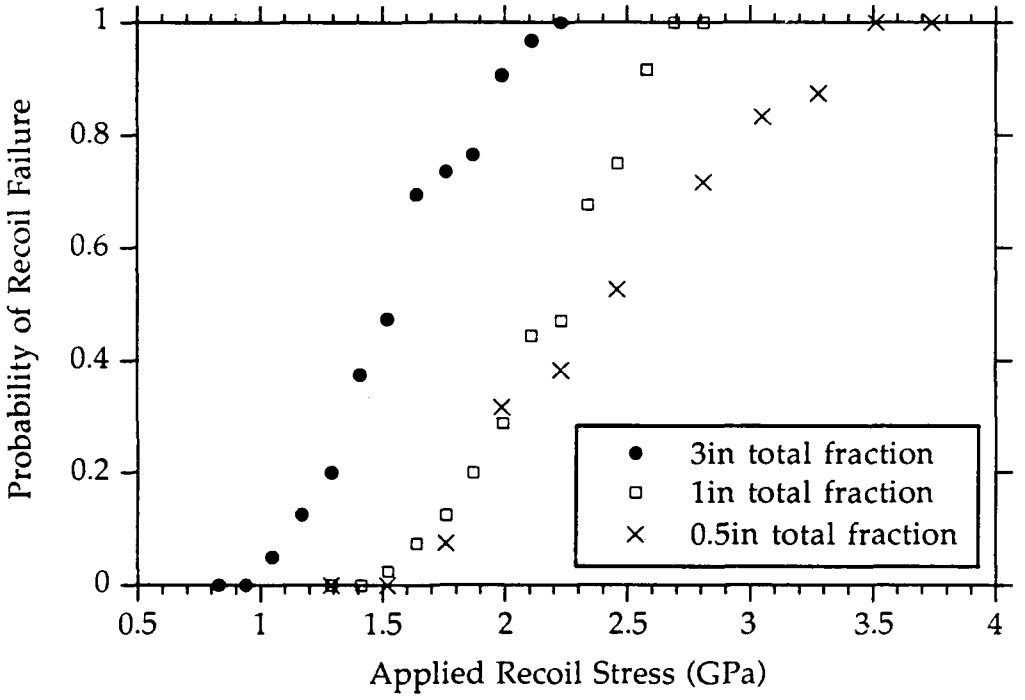
Probability of Recoil Failure
1
0.8
0.6
0.4
0.2
0
0.5
1
1.5
2
2.5
3
3.5
4
Applied Recoil Stress (GPa)
3in total fraction
1in total fraction
0.5in total fraction

Fig. 3

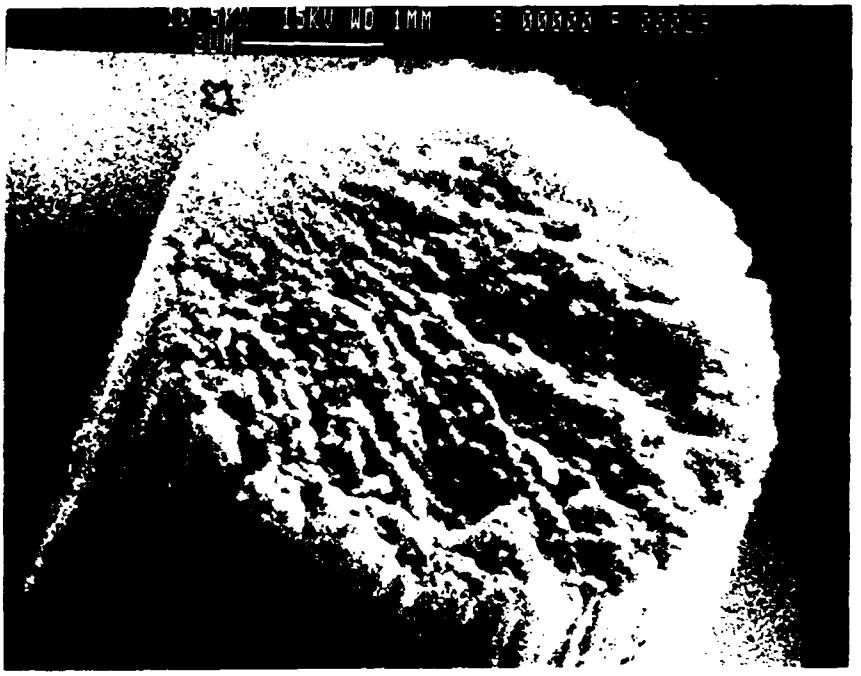

A

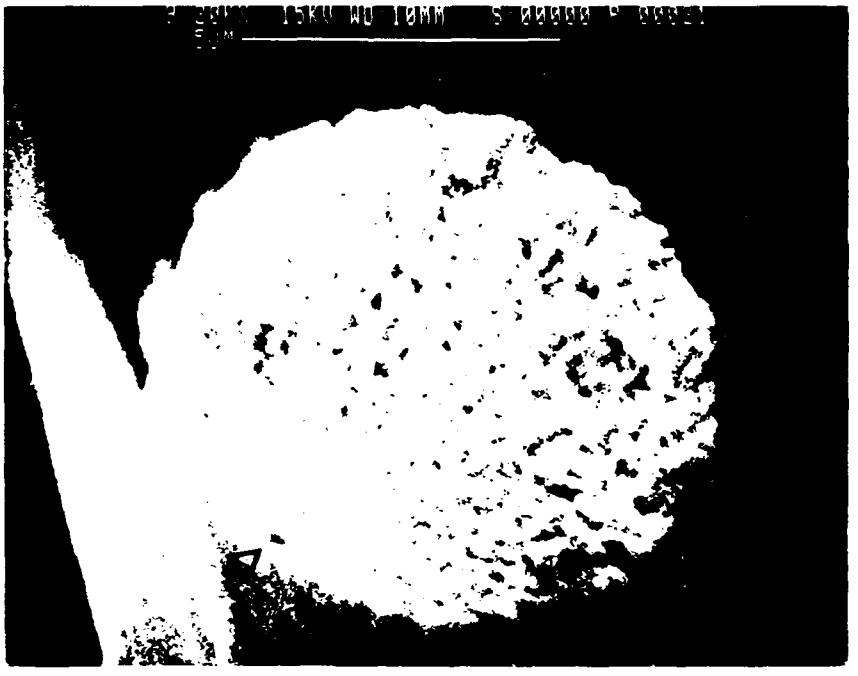

B

Fig. 4

A

B

Fig. 5

Fig. 6

Fig. 1

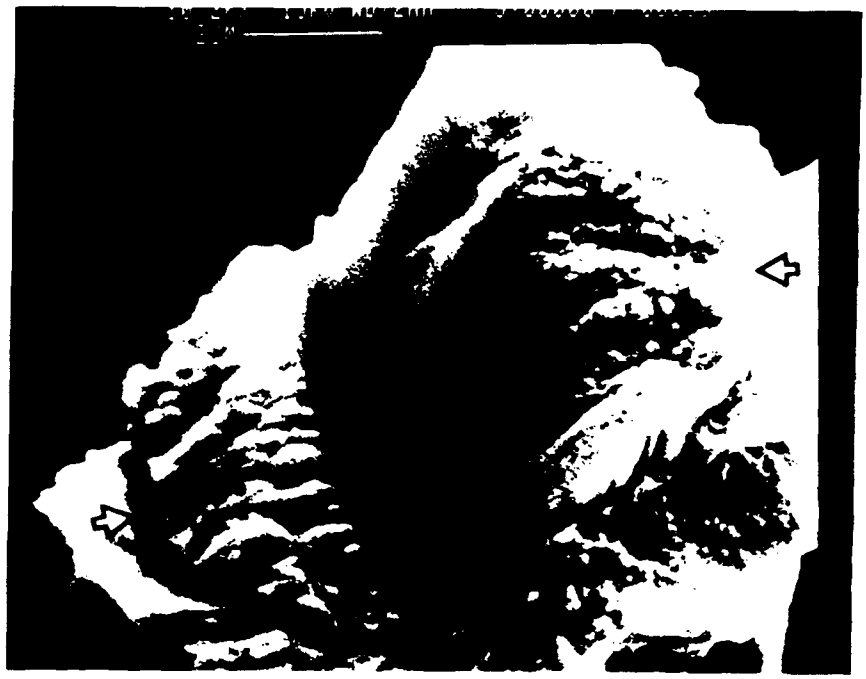

A

B

Fig. 8

Fig. 9

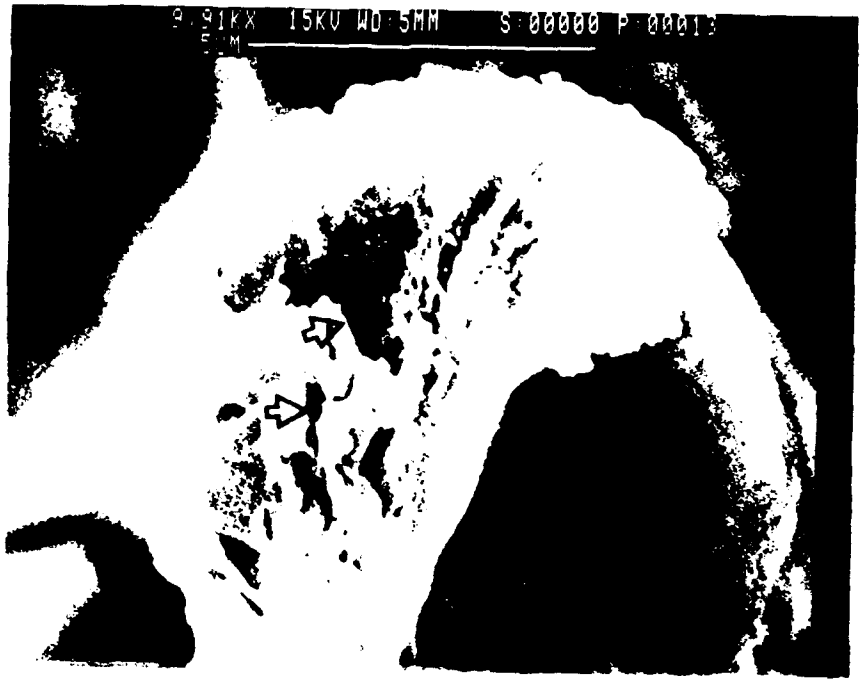

Fig. 10

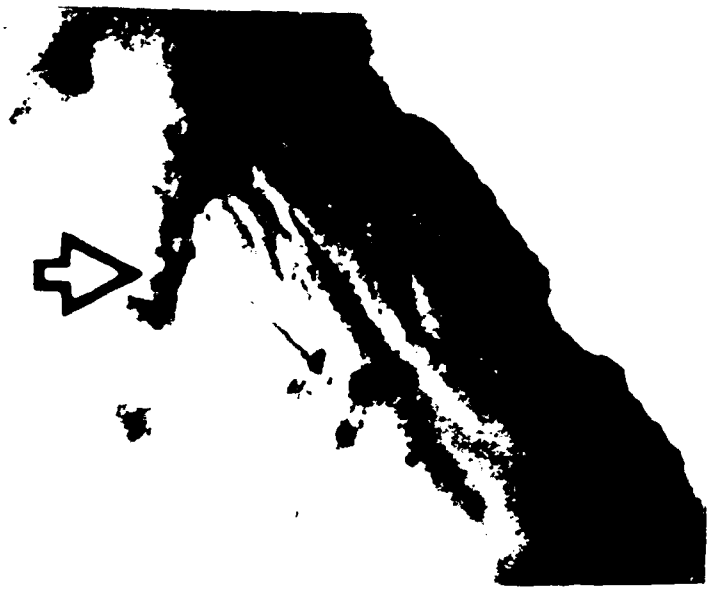

Fig. 11

A

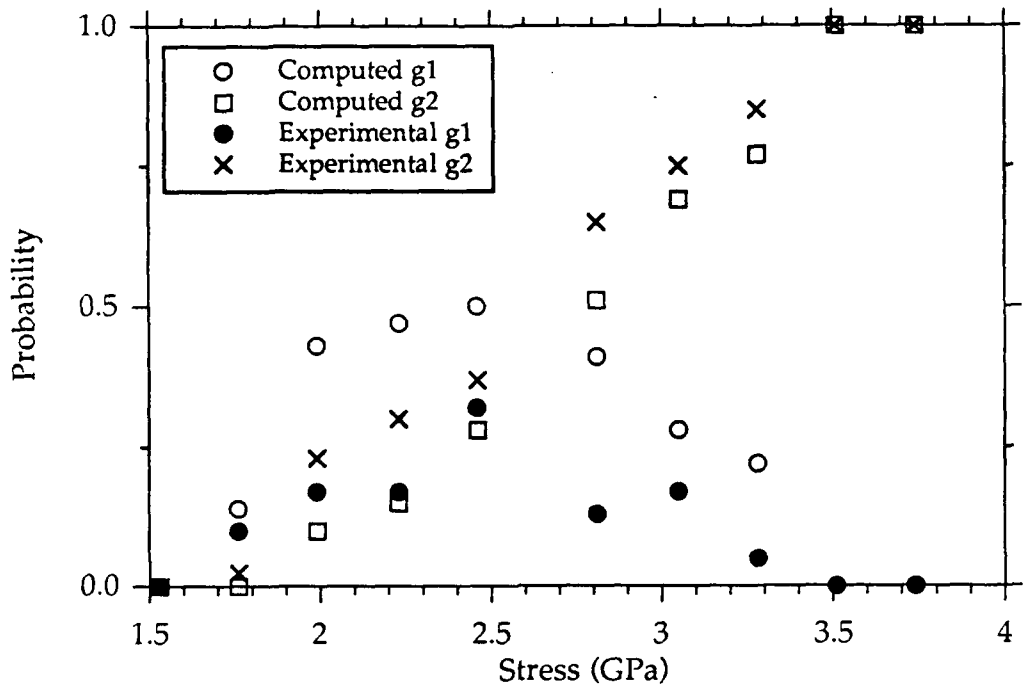
Computed g1
Computed g2
Experimental g1
Experimental g2
Probability
1.0
0.5
0.0
1.5
2
2.5
3
3.5
4
Stress (GPa)

B

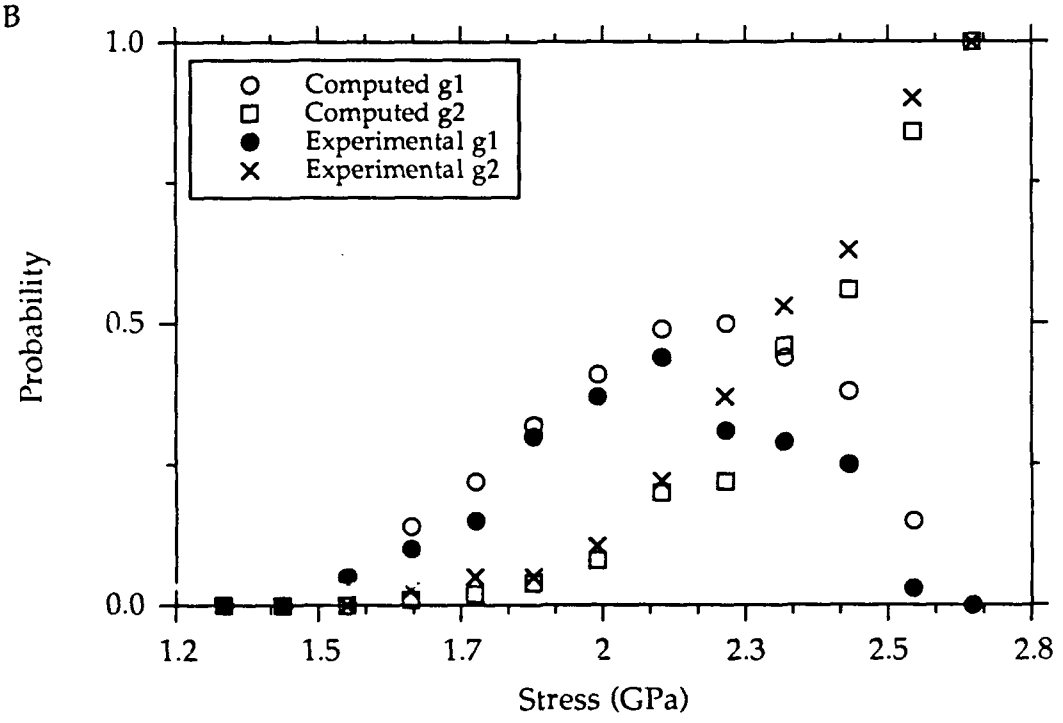
Computed g1
Computed g2
Experimental g1
Experimental g2
Probability
1.0
0.5
0.0
1.2
1.5
1.7
2
2.3
2.5
2.8
Stress (GPa)

C

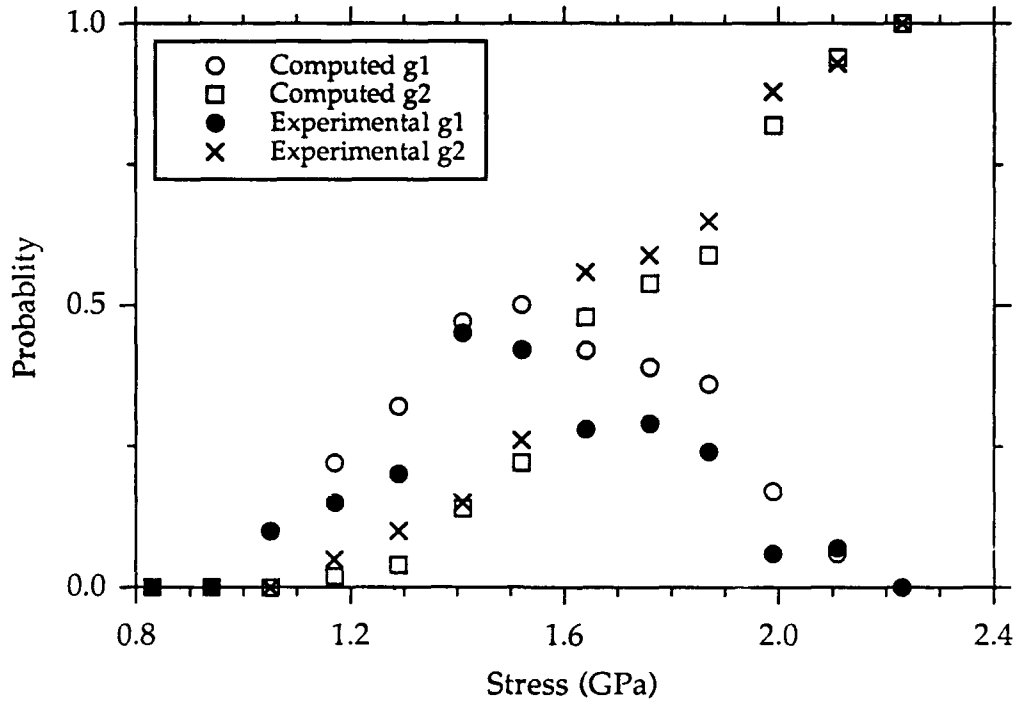
Computed g1
Computed g2
Experimental g1
Experimental g2
Probablity
1.0
0.5
0.0
0.8
1.2
1.6
2.0
2.4
Stress (GPa)

Fig. 12

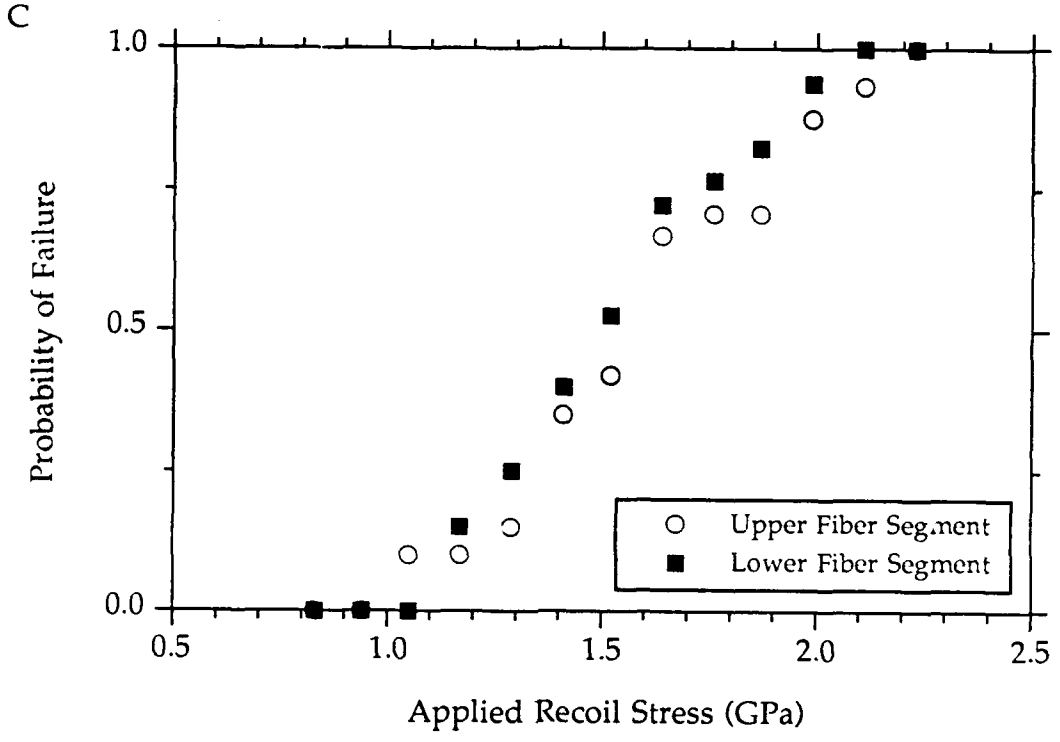
C
1.0
0.5
0.0
Probability of Failure
0.5
1.0
1.5
2.0
2.5
Applied Recoil Stress (GPa)
Upper Fiber Segment
Lower Fiber Segment

Fig. 13

A

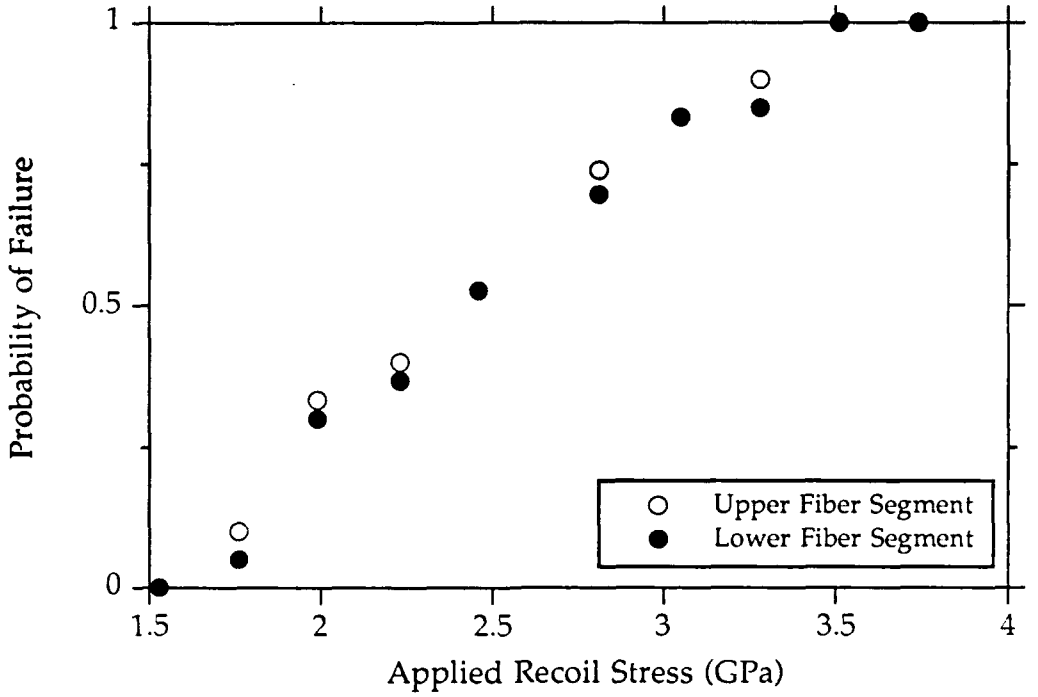
1
0.5
0
Probability of Failure
Upper Fiber Segment
Lower Fiber Segment
1.5
2
2.5
3
3.5
4
Applied Recoil Stress (GPa)

B

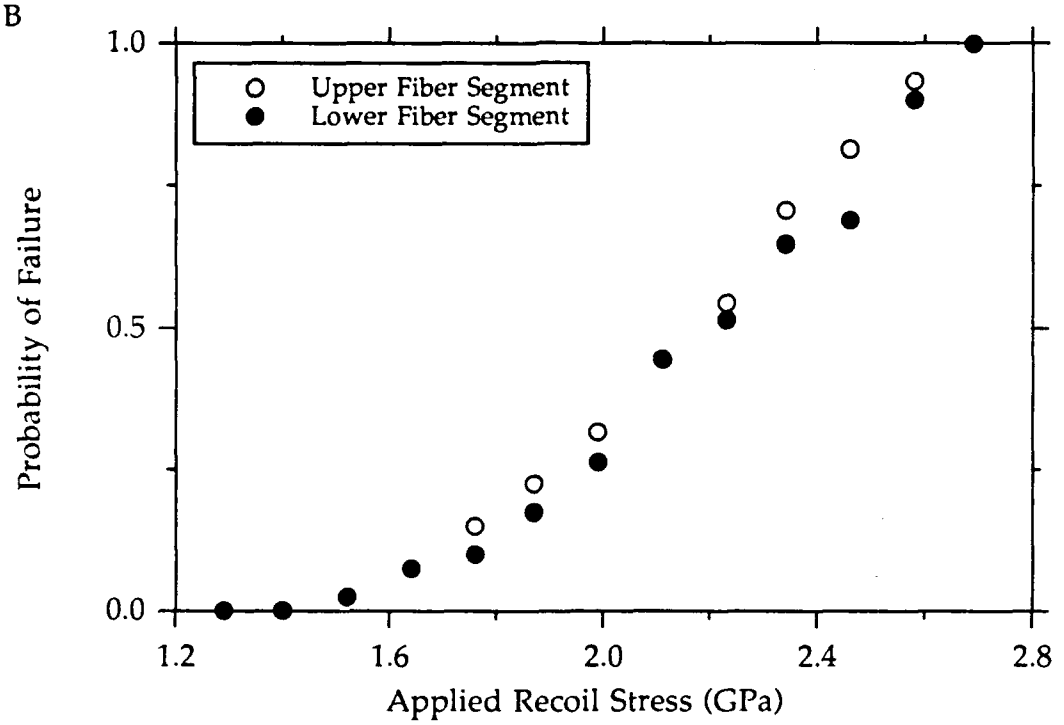
1.0
0.5
0.0
Probability of Failure
Upper Fiber Segment
Lower Fiber Segment
1.2
1.6
2.0
2.4
2.8
Applied Recoil Stress (GPa)

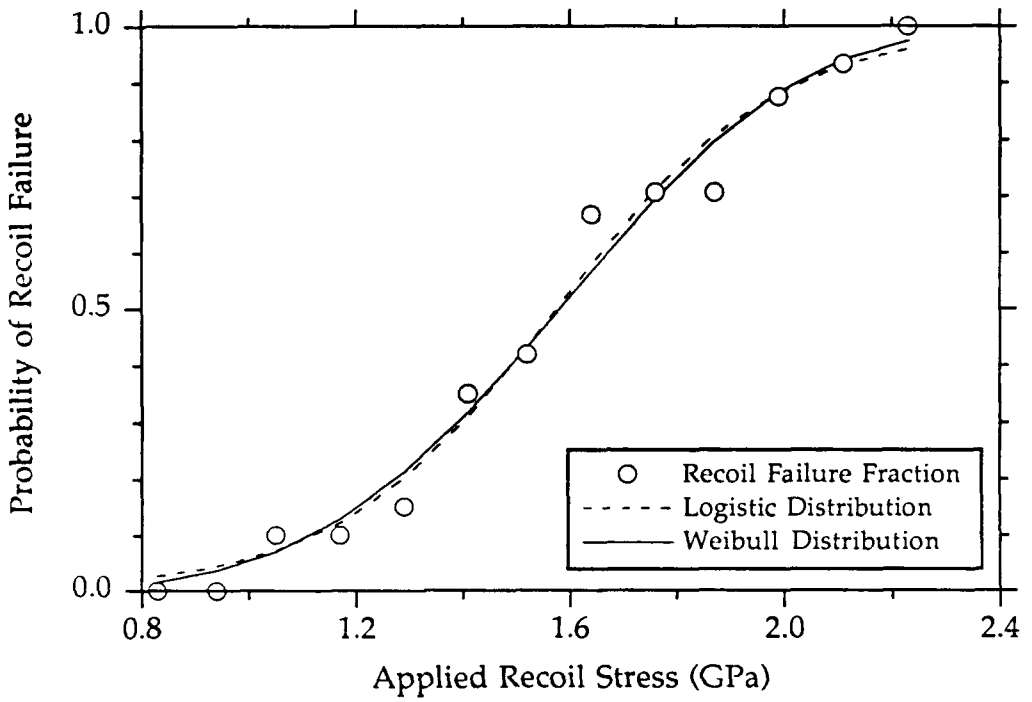
1.0
0.5
0.0
Probability of Recoil Failure
0.8
1.2
1.6
2.0
2.4
Applied Recoil Stress (GPa)
Recoil Failure Fraction
Logistic Distribution
Weibull Distribution

Fig. 14

A

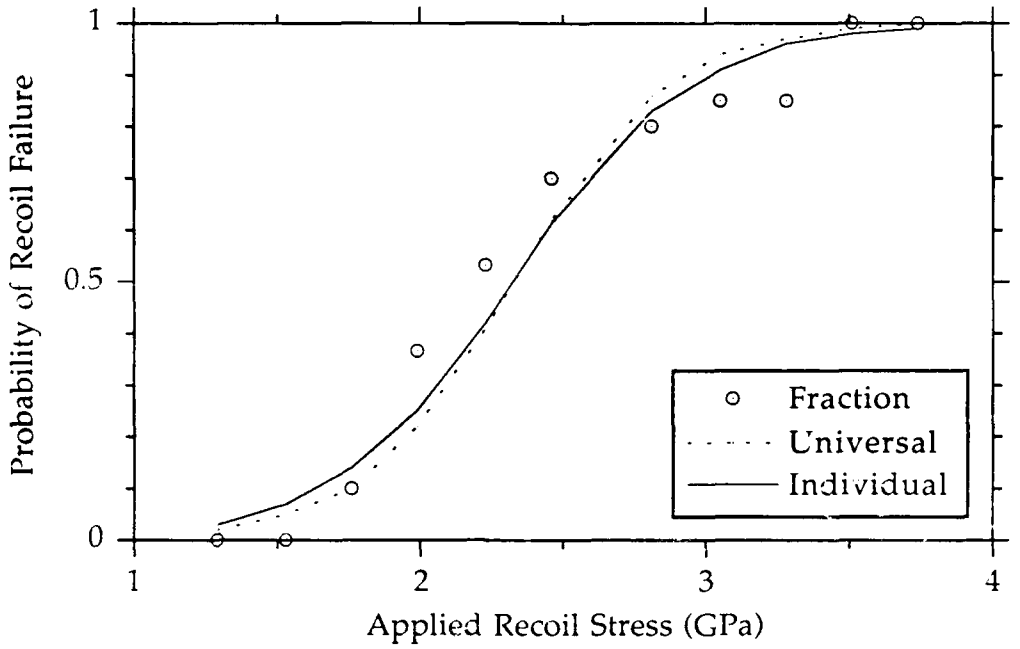
Probability of Recoil Failure
1
0.5
0
1
2
3
4
Applied Recoil Stress (GPa)
Fraction
Universal
Individual

B

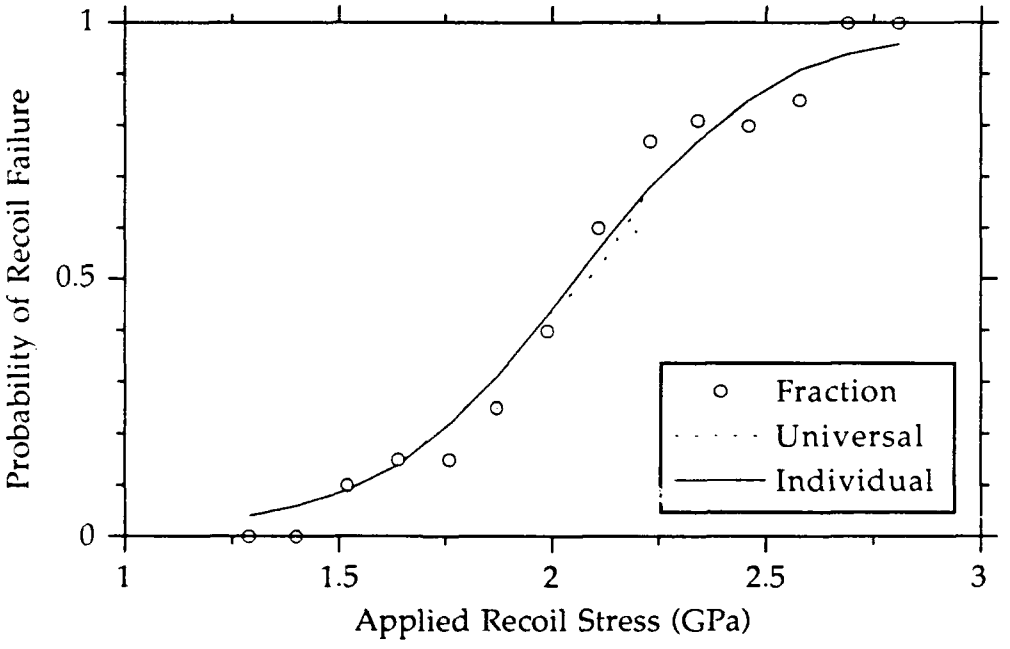
Probability of Recoil Failure
1
0.5
0
1
1.5
2
2.5
3
Applied Recoil Stress (GPa)
Fraction
Universal
Individual

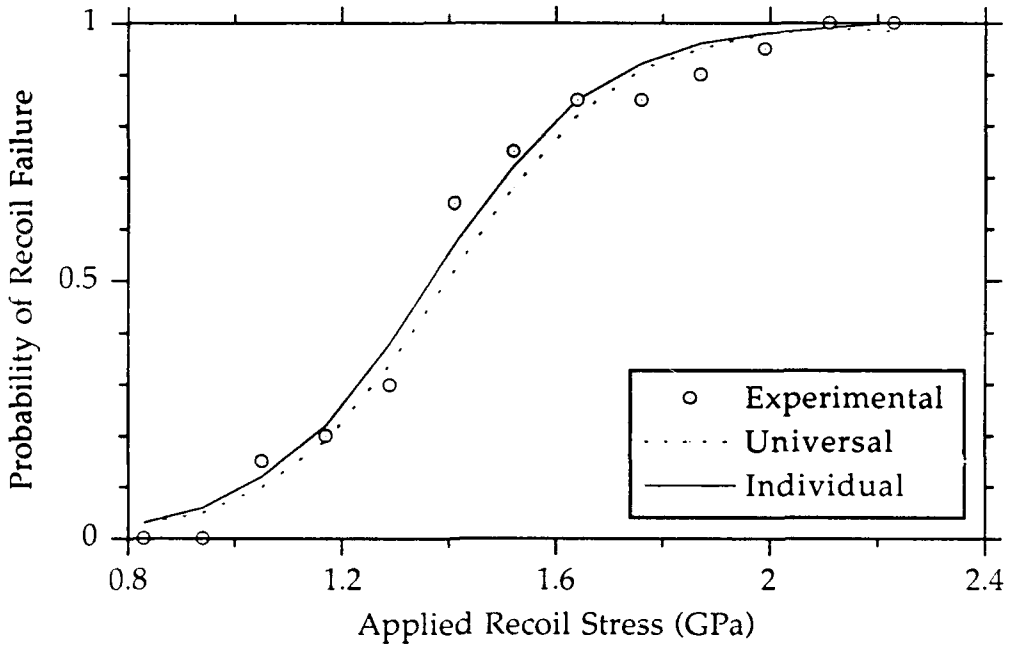
1
0.5
0
Probability of Recoil Failure
0.8
1.2
1.6
2
2.4
Applied Recoil Stress (GPa)
Experimental
Universal
Individual

Fig. 15